

1 **Reply to Referee #1:**

2 We deeply appreciate your helpful comments and suggestions, which enabled us to improve
3 the quality of our present study. In our response, we use italicization in blue to indicate the
4 reviewer's comments, and normal type in black for our response. Besides, we use boldface
5 type to indicate changes in the manuscript.

6 **General comments:**

7 *One additional analysis that I would like to see is a comparison among BECs per species. This*
8 *would help show how each BEC constrains the spreads vertically and horizontally around the*
9 *observation sites. Similar analyses are described in below:*

10 *Descombes, G., Auligné, T., Vandenberghe, F., Barker, D. M. and Barré, J.: Generalized*
11 *background error covariance matrix model (GEN_BE v2.0), Geosci. Model Dev., 8(3), 669–*
12 *696, doi:10.5194/gmd-8-669-2015, 2015.*

13 *Liu, Z., Liu, Q., Lin, H.-C., Schwartz, C. S., Lee, Y.-H. and Wang, T.: Three-dimensional*
14 *variational assimilation of MODIS aerosol optical depth: Implementation and application to*
15 *a dust storm over East Asia: AOD DATA ASSIMILATION, Journal of Geophysical Research:*
16 *Atmospheres, 116(D23), doi:10.1029/2011JD016159, 2011.*

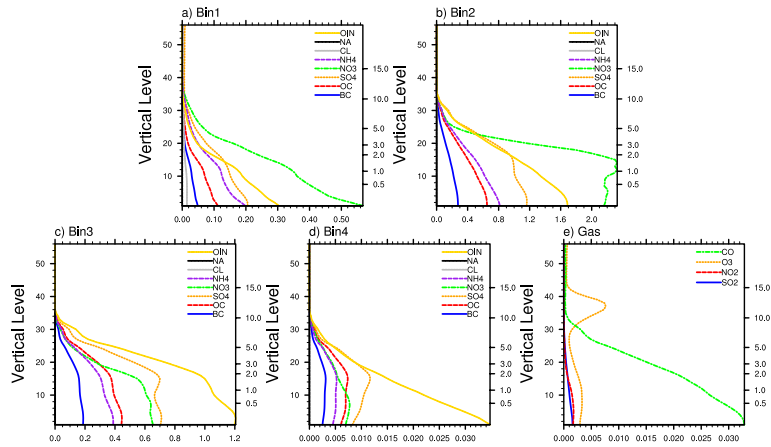
17 **Response:**

18 Accepted. Following the references above, a comparison among the BECs per species has
19 been added in the manuscript with a new figure as Figure 2, which shows the background error
20 standard deviations. Also, analyses about the background error horizontal correlation length
21 scales and vertical correlation have been mentioned in the manuscript with figures shown here
22 as Figures R1 and R2 (not shown in the manuscript). The analyses are presented in section
23 2.3.3 in the manuscript as below.

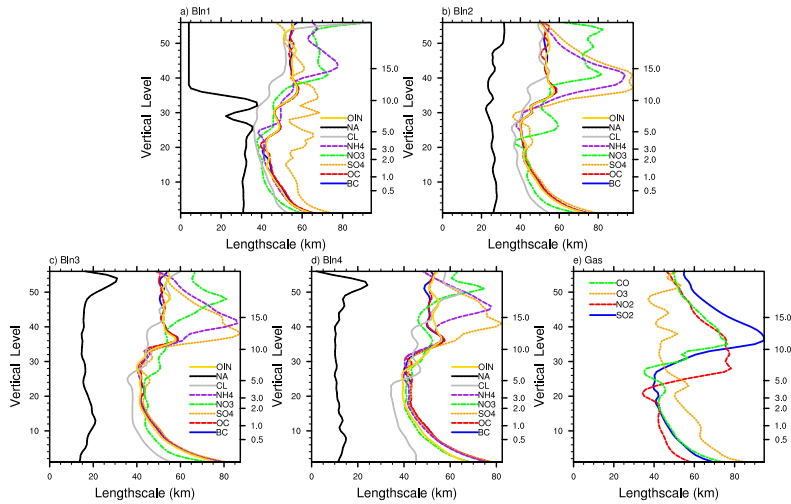
24 **“Following the analyses based on the GEN_BE v2.0 (Descombes et al. 2015), Figure**
25 **2 presents the background error standard deviations of each species at different vertical**
26 **levels. For the aerosols in the first three size bins (Fig. 2a-2c), although the standard**
27 **deviation errors vary across the species, the errors of NO_3^- , SO_4^{2-} , NH_4^+ , OC, and OIN**
28 **are generally larger than that of the others (BC, CI and NA) in the three size bins. These**
29 **results are consistent with the finding in Chen et al. (2019), which allows inorganic**
30 **compounds (NO_3^- , SO_4^{2-} , NH_4^+), OC and OIN to be adjusted more in corresponding to**
31 **their larger background errors. For the aerosols in the 4th size bin (Fig. 2d), the errors**
32 **are unreasonably much smaller than that in the first three bins due to model deficiency.**
33 **Under this circumstance, to get a reasonable bigger adjustment for the aerosols in the 4th**

34 size bin, it might need to enlarge their background errors in the DA procedure. As for the
35 gaseous pollutants (Fig. 2e), CO has the biggest background errors in the middle and
36 lower layers, followed by O3, SO2 and NO2.

37 For the background error horizontal correlation length scales, the results are similar
38 as in Liu et al. (2011) (figure omitted). The length scales of aerosols are comparable in
39 most of the species, which generally span from 1.5 to 2.5 times the grid spacing, while the
40 aerosol species NA exhibits a smaller horizontal length scale than all the other species.
41 For the background error vertical correlations (figure omitted), the results are similar as
42 in Descombes et al. (2015), in which the vertical correlations are bigger in the lower levels
43 (where they are emitted) in most of the species. According to Descombes et al. (2015), the
44 reactions with species emitted near the surface might create these strong correlations in
45 the lower model levels.”

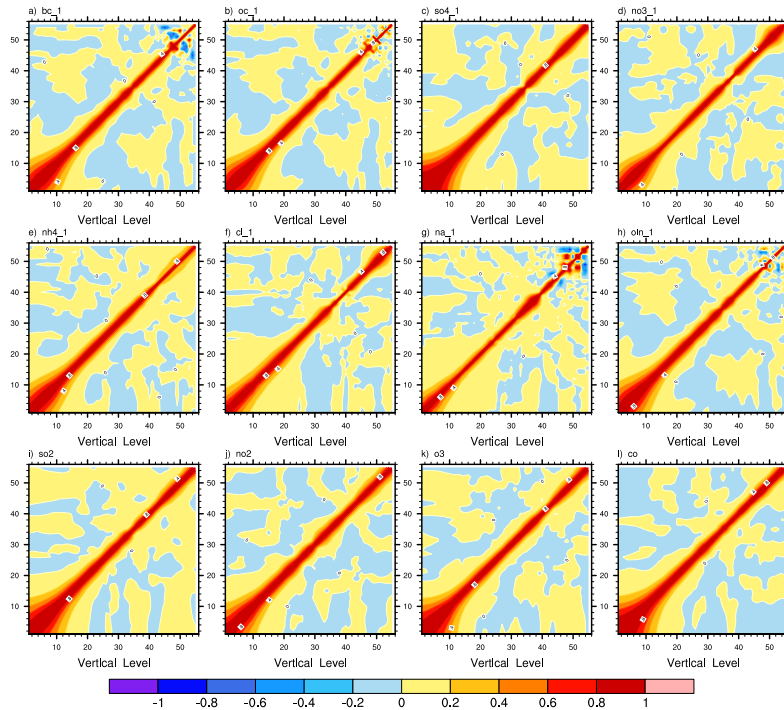


46
 47 **Figure 2. Background error standard deviations of aerosol species in the (a) 1st size bin,**
 48 **(b) 2nd size bin, (c) 3rd size bin, (d) 4th size bin, and of (e) gas pollutants. The units for**
 49 **the x-axis are $\mu\text{g m}^{-3}$ for (a)-(d) and ppm for (e). The left y-axis denotes the model level,**
 50 **and the right y-axis denotes the vertical height (units: km).**



51
 52 **Figure R1. Background error horizontal correlation length scales of aerosol species in the (a)**

53 1st size bin, (b) 2nd size bin, (c) 3rd size bin, (d) 4th size bin, and of (e) gas pollutants (units:
54 km). The left y-axis denotes the model level, and the right y-axis denotes the vertical height
55 (units: km).



56
57 Figure R2. Background error vertical correlation of aerosol species in the (a-h) 1st size bin,
58 and of (i-l) gas pollutants. The left x-axis and y-axis denote the model level.

59
60 **Other minor issues:**

61 *1. Please present other emissions such as dust, biogenic and fire emission used in your study.*

62 Response:

63 Accepted. The description of the corresponding emissions has been listed in section 2.1 in
64 the manuscript as below.

65 **“The dust emission is the GOCART dust emission and the biogenic emission is**
66 **calculated online by the Gunther scheme within the WRF-Chem model. Given the time**
67 **period of this study (January) is not the period with massive fires (crop/biomass burning),**
68 **the fire emission is not used in this study.”**

69

70 *2. Please describe the reason why cross correlations were not applied.*

71 Response:

72 The statement related to the cross-correlation issue, “Cross-correlations between different
73 aerosol/chemical variables were not considered”, has been replaced in the manuscript as below.

74 **“Since it is both technically and scientifically challenging to model the cross-**
75 **correlations between different aerosol/chemical variables in a 3DVAR framework, they**
76 **are not considered in this study. We plan to introduce the cross-variable correlations with**

77 **the ensemble-variational approach in the future extension of the system.”**

78

79 *3. Could you describe the other trials for the background error covariance of the PM-coarse?*

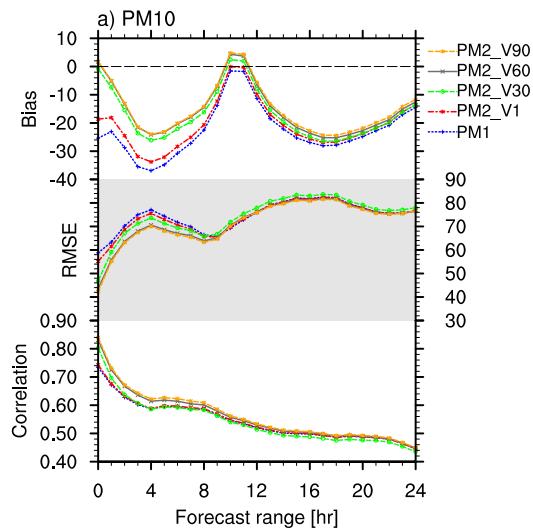
80 *Did the inflation factor of 90 was applied along with all vertical levels?*

81 Response:

82 The inflation for the background error covariance is actually controlled by a new
83 “var_scaling” factor similar as the original “var_scaling” for meteorology assimilation in
84 WRFDA, and thus the inflation factor of 90 is currently applied to all the vertical levels similar
85 as the inflation in meteorology assimilation.

86 Regarding the other trials for the background error covariance, the statistics of PM₁₀ in the
87 forecast are presented by Fig. R3 as below (not included in the manuscript). Since the trials are
88 for the background error covariance of the PMcoarse, the statistics for PM_{2.5} and gaseous
89 pollutants are highly similar among the trials and thus are not shown. The PM2_V1, PM2_V30,
90 PM2_V60, and PM2_V90 are the experiments assimilating PMcoarse and PM_{2.5}
91 simultaneously but with PMcoarse inflation factor of 1, 30, 60, and 90 respectively through
92 the setting of “var_scaling” (the PM_{2.5} inflation factor all kept 1); the PM1 experiment is the

93 same one as in the manuscript that only assimilate the $PM_{2.5}$. Without the inflation, the
94 $PM2_V1$ experiment are close to the $PM1$ experiment, which suggests that assimilating
95 PM_{coarse} without inflation does not bring significant improvements to the forecast of PM_{10}
96 as originally expected. Therefore, as stated in the manuscript, the inflation factor is used to
97 address this issue. Viewing from Fig. R3, the forecast PM_{10} generally improves with the
98 enlargement of the inflation factor, especially for the forecast range within 0-9 hr. This result
99 is corresponded to the analysis of Fig. 4 in the manuscript, suggesting that it could be better to
100 enlarge the background error covariance of the PM_{coarse} . Given the $PM2_V90$ experiment
101 exhibits the best forecast performance, and $PM2_V90$ is relatively close to $PM2_V60$, the
102 inflation factor of 90 is finally used in the manuscript without further enlargement.



103

104 **Figure R3.** Averaged bias (units: $\mu\text{g}/\text{m}^3$), RMSE (units: $\mu\text{g}/\text{m}^3$), and correlation for PM_{10} in
 105 different experiments as a function of forecast range, verified against the surface observations
 106 of 531 stations in China. The blue, red, green, gray, and orange lines denote the results of
 107 experiment PM1, PM2_V1, PM2_V30, PM2_V60, and PM2_V90, respectively.

108

109 **Specific minor issues:**

110 *Page 1. line 20: SO2 and CO -> SO2, and CO*

111 Corrected.

112 *Page 3. line 42: fastest growing -> fastest-growing*

113 Corrected.

114 *Page 3. line 43: extreme haze -> the extreme haze*

115 Corrected.

116 *Page 4. line 58: scientific community -> the scientific community*

117 Corrected.

118 *Page 5. line 87: treatment -> treatments*

119 Corrected.

120 *Page 6. line 102: data assimilation -> DA*

121 Corrected.

122 *Page 6. line 108: recent -> recently*

123 Corrected.

124 *Page 6. line 113: extend -> extent or extends?*

125 Accepted. The word “extend” has been revised to “extent” in the manuscript.

126 *Page 6. line 116: observations and -> observations, and*

127 Corrected.

128 *Page 7. line 123: brief summary -> summary (tautology)*

129 Accepted. The phrase “brief summary” has been revised to “summary” in the manuscript.

130 *Page 8. line 151: capability -> the capability*

131 Corrected.

132 *Page 10. line 197: PM25 are -> PM25 is*

133 Corrected.

134 *Page 11. line 205: in first -> in the first*

135 Corrected.

136 *Page 12. line 233: each of the aerosoll/chemical variable -> each of the aerosoll/chemical*

137 *variables*

138 Corrected.

139 *Page 13. line 253 – 256: needed to be tailored more clearly*

140 The corresponding statement has been revised in the manuscript as below.

141 **“In view of the cycling frequency is an important aspect in the DA strategy, especially**

142 **for 3DVAR, two more experiments that assimilate all the six major pollutants with 3-h**

143 **and 1-h cycling frequency are conducted respectively (experiment ALL_3h and**

144 **ALL_1h).”**

145 *Page 15. Line 295: is slightly larger -> are slightly larger*

146 Corrected.

147 *Page 16. line 303: Due to lack -> Due to the lack*

148 Corrected.

149 *Page 16. line 305: As show -> As shown*

150 Corrected.

151 *Page 16. line 308: among -> to*

152 Corrected.

153 *Page 16. line 316: including bias, RMSE and correlation -> including bias, RMSE, and*

154 *correlation*

155 Corrected.

156 *Page 16. line 318: model -> the model, poor -> poorly*

157 Corrected.

158 *Page 17. line 322: percentage -> percentages*

159 Corrected.

160 *Page 17. line 328: lead -> leads*

161 Corrected.

162 *Page 17. line 329: individual -> the individual*

163 Corrected.

164 *Page 17. line 330: general -> generally*

165 Corrected.

166 *Page 18. line 346: applications, but also -> applications but also*

167 Corrected.

168 *Page 18. line 362, Page 19. Line 364, and Page 21. Line 425: heavy -> heavily*

169 Corrected.

170 *Page 19. line 379: ALL_3h and ALL_1h -> ALL_3h, and ALL_1h*

171 Corrected.

172 *Page 20. line 397: becomes -> become*

173 Corrected.

174 *Page 20. line 403: determine -> determines*

175 Corrected.

176 *Page 21. line 411: SO2 and CO -> SO2, and CO*

177 Corrected.

178 *Page 25. line 508: study -> a study*

179 Corrected.

180 *Page 25. line 509: contains -> contain*

181 Corrected.

182

183 **Reply to Referee #2:**

184 We deeply appreciate your helpful comments and suggestions, which enabled us to improve
185 the quality of our present study. In our response, we use italicization in blue to indicate the
186 reviewer's comments, and normal type in black for our response. Besides, we use boldface
187 type to indicate changes in the manuscript.

188 **Specific Comments:**

189 *1. Page 14, Line 267: Can you provide possible reasons why the model significantly*
190 *underestimated PMcoarse? Missing emissions?*

191 Response:

192 Yes, missing emissions could be the major reason for the underestimated PMcoarse
193 simulation in the model. Different from the United states or European countries that national
194 emission inventories are provided and updated frequently by the government (e.g. US National
195 Emission Inventory NEI 05-08-11-14-17), the publicly available emission inventories for
196 China are mainly established by several scientific research groups. In the US, NEI are
197 established based upon data provided by state, local, and tribal air agencies for sources in their
198 jurisdictions and are supplemented by data that developed by the US Environmental Protection
199 Agency; thus the statistics are comprehensive and detailed. In China, the scientific research

200 groups established EIs only by public released statistics of energy, activity, emission factor etc.,
201 which are usually limited and incomplete; thus the uncertainties of the publicly available
202 emission inventories in China are relatively larger compared with others (US, European
203 countries). It's a known problem that the fugitive dust emissions over the whole of China is
204 still lack, which might cause the underestimated PMcoarse simulation in the model.

205 Some related statements have also been added in the discussion section of the manuscript
206 as below.

207 **“As for the significantly underestimated PMcoarse in the model, the results might**
208 **relate to the missing emissions under current situations. Different from the United states**
209 **or European countries that national emission inventories are provided and updated**
210 **frequently by the government (e.g. US National Emission Inventory NEI 05-08-11-14-17),**
211 **the publicly available emission inventories for China are mainly established by several**
212 **scientific research groups. In result, the uncertainties of the publicly available emission**
213 **inventories in China are relatively larger compared with others (US, European countries),**
214 **and it's a known problem that the fugitive dust emissions over the whole of China is still**
215 **lack, which might cause the underestimated PMcoarse simulation in the model.”**

216

217 *2. Page 16, Line 305: Does Figure 4 show the vertical profiles of pollutant concentrations in*

218 *the model simulations? It is not clear why the ozone levels are so low in the upper troposphere*

219 *(9 km or above 15 km). Does the model account for stratospheric ozone boundary conditions?*

220 *Please clarify.*

221 Response:

222 Yes, Figure 4 (updated as Figure 5 in the manuscript) shows the vertical profiles of

223 pollutants concentrations in the model simulations. Thanks for the kind reminder! The

224 stratospheric ozone boundary conditions are not taken into account, which might be the reason

225 for the low ozone level in upper tropopause.

226

227 *3. Page 18, Line 356-360: I suggest move the definition of the threat score (TS) from the*

228 *Supplement to the main text here. Also here in the text I suggest explain what the values of TS*

229 *represent.*

230 Response:

231 Accepted. The definition and explanation of the threat score (TS) have been moved from

232 the supplement to the manuscript as below.

233 **“To reflect the integrated DA effect of aerosols and gas-phase pollutants, the threat**
234 **score (TS), one of the most commonly used criteria in the verifications of**
235 **meteorological forecasts, is used for Air Quality Index (AQI) for six AQI levels. The**
236 **threat score (TS) for AQI is calculated by**

237
$$TS_i = \frac{H_i}{H_i + M_i + F_i} \quad (6)$$

238 **where H, M, and F denote the counts of the hits, the misses, and the false alarms in the**
239 **forecast of AQI, and i denotes the AQI levels from 1 to 6. In result, the TS is acquired at**
240 **each AQI level ranging from 0 to 1, and the higher (lower) TS represents the better (worse)**
241 **forecast performance.”**

242

243 *4. Page 19, Line 379: Need to explain here “ALL_6h” is the “ALL” simulation in Table 2,*
244 *right?*

245 Response:

246 Accepted. The “ALL_6h” is the “ALL” experiment in Tab.2, and the explanation has been
247 added in the manuscript as below.

248 **“Figure 9 shows the domain-averaged bias and RMSE of the analysis as in Fig. 3, but**
249 **for experiments with different DA frequencies (ALL_6h, ALL_3h, and ALL_1h; the**
250 **ALL_6h is the ALL experiment in Tab.2).”**

251

252 *5. Page 20, Line 397-406:I do not think the discussion on ozone performance here and other*
253 *places (e.g., abstract, conclusions) is convincing. The study also simulated a winter month*
254 *(January 2017) when ozone photochemistry is very weak. Therefore, I do not think that the*
255 *ozone photochemistry or NOxVOC ratios would explain the decreased forecast skill for ozone*
256 *when increasing assimilation frequency. Since January is not an ozone pollution season, the*
257 *conclusion that “assimilate O3 and NO2 every 6 h” would not be robust only based on results*
258 *of this month. Please clarify and discuss the limits.*

259 Response:

260 Accepted. Thanks for the great suggestion! It could possibly also be related with the NO_x
261 titration due to the changed NO₂ concentrations. The discussion on the ozone performance in
262 association with NO₂/VOC ratios has been weakened in the manuscript, the abstract, and the
263 conclusion as below. The discussion on NO_x titration is added, and the limits of the current

264 findings are also mentioned in the discussion section.

265 *Statements in section 3.3 of the manuscript:*

266 **“However, the analysis and 24-hr forecast of O₃ become worse under higher cycling**
267 **frequencies for this winter season (Fig. 9e and 11c). Given the analysis is at 00 UTC, the**
268 **worsen analysis in the experiments with higher DA frequencies (1-h, 3-h) could be mainly**
269 **due to the unfavorable changes in the 1-h/3-h forecasts period (starting from 23 UTC, 21**
270 **UTC), which is different from the situation in the 6-h cycling experiment. As for the**
271 **forecasts, the 24-hr performances starting from 00 UTC show complex changes along**
272 **with the forecast range: compared to the 6-h cycling experiment, the biases in the**
273 **experiments with higher DA frequencies decrease at 09-14 UTC but increase for other**
274 **hours; the RMSE and correlations in the experiments with higher DA frequencies become**
275 **worse in most of the hours (Fig. 11c). It should be mentioned that O₃ is a relatively short-**
276 **lived chemical reactive species, and takes part in highly complex and photochemical**
277 **reactions in association with NO_x and VOC (Peng et al. 2018, Lu et al., 2019). From this**
278 **perspective, the performances of O₃ could also rely on the photochemistry and the NO_x**
279 **titration, in addition to the IC. Although the winter month (January 2017) is investigated**

280 here when ozone photochemistry is relatively weaker compared to other seasons, the
281 photochemistry and the NO_x titration still play their roles. Accordingly, when the
282 assimilation of NO₂ changes the NO₂ concentration and leave the NO and VOC
283 unadjusted due to the absence of NO and VOC measurements, two results might occur:
284 firstly, the NO₂/VOC ratio which determine the photochemical reactions and even the
285 regime might be changed (O₃ production/loss direction might change); secondly, the NO_x
286 titration process might be changed due to the NO₂ concentration updates (but no change
287 on NO). Considering the relevant NO_x-VOC-O₃ reactions take place quickly, changing
288 the O₃ concentration in a short period, the advantage of IC DA could compete with the
289 disadvantages of the disordered photochemistry (inaccurate NO₂/VOC ratios) or the
290 changed titration (adjusted NO₂ concentrations but not NO) resulting from the DA.
291 Under this circumstance, the more frequent the O₃ and NO₂ were assimilated, the more
292 incompatibilities could be brought into the related photochemical/titration reactions,
293 resulting the model performs worse in the O₃ forecasts under higher cycling frequencies.
294 It is noted that these statistics were only for the analysis at 00UTC and the 24-hr forecast
295 starting from 00UTC for winter season. Since O₃ has strong diurnal and seasonal

296 variations, more experiments and statistics at different time of the day and different
297 season of the year should be conducted in the future.”

298 *Statements in the abstract:*

299 “For O₃, although improvements are acquired at the 6-h cycling frequency, the
300 advantage of more frequent DA could be consumed by the disadvantages of the
301 unbalanced photochemistry (due to inaccurate precursor NO_x/VOC ratios) or the
302 changed titration process (due to changed NO₂ concentrations but not NO) from
303 assimilating the existing observations (only O₃ and NO₂, but no VOC and NO); yet the
304 finding is based on the 00 UTC forecast for this winter season only and O₃ has strong
305 diurnal and seasonal variations, more experiments should be conducted to draw further
306 conclusions.”

307 *Statement in the conclusion:*

308 “for O₃, compared to a better performance at the 6-h cycling frequency, its analysis
309 at 00 UTC and the following 24-hr forecast become generally worse under higher cycling
310 frequencies for this winter season, although the biases did decrease at 09-14 UTC in the
311 24-hr forecast. Considering the relevant NO_x-VOC-O₃ reaction system changes the

312 **NO₂/O₃ concentration in a short period, the advantage of IC DA could compete with the**
313 **disadvantages of the disordered photochemistry (inaccurate NO₂/VOC ratios) or the**
314 **changed titration (adjusted NO₂ concentrations but not NO) resulting from the DA. In**
315 **future applications, it is better to assimilate PM_{2.5}, PM₁₀, SO₂, and CO every 1 h. For the**
316 **frequency of O₃ and NO₂ assimilation, every 6 h is the best in this winter season in our**
317 **study. Since O₃ has strong diurnal and seasonal variations, more experiments and**
318 **statistics at different time of the day and different season of the year should be conducted**
319 **in the future. Also, it might be helpful to assimilate NO/VOC simultaneously with O₃ and**
320 **NO₂ after there are corresponding measurements.”**

321

322 *6. Page 23, Line 460-462: As a future development, is it possible to directly constrain the*
323 *coefficients of heterogeneous reactions using the data assimilation system?*

324 Response:

325 Yes. The variables in the heterogeneous reactions include precursor concentrations,
326 meteorology (RH), and uptake coefficients. Two DA approaches would be tried in the future
327 to fully utilize the observations and constrain uptake coefficients.

328 The first approach is by the 3DVAR technique: (1) simultaneously assimilate precursor
329 concentrations and meteorology (RH) in the model to generate the best initial condition (IC);
330 (2) start from this IC, conduct sensitivity simulations with a series of adjusted uptake
331 coefficients to best match the SNA species observations.

332 The second approach is by the Ensemble Kalman Filter (EnKF) technique which might be
333 computing expensive: (1) perturb the uptake coefficients in the model and generate ensemble
334 members through model forecasts; (2) use all observations (precursor concentrations, RH,
335 species) in the EnKF system as constraints to optimize the uptake coefficients.

336

337 *7. Page 50, Figure 12: Need to add the unit in the figure or in the caption.*

338 Response:

339 Accepted. The units have been added in the caption of the figure, and the figure number
340 has been updated as 13.

341

342 *8. Page 51, Figure 13: The titles say "Used 79" and "Used 80". What do they mean?*

343 Response:

344 They are the accumulated numbers of the used observations around Beijing area during
345 January 16 (1600 UTC, 1606 UTC, 1612 UTC, and 1618 UTC). The corresponding description
346 has been added in the caption in the manuscript as below, and the figure number has been
347 updated as 14.

348 **“Figure 14. Averaged scatter plot of (a, c) observation versus background and (b, d)**
349 **observation versus analysis for (a, b) SO₂ and (c, d) NO₂ around Beijing area (red dots in**
350 **Fig. 1) on January 16. The numbers on the title denote the accumulated numbers of the**
351 **used observations around Beijing area during January 16 (1600 UTC, 1606 UTC, 1612**
352 **UTC, and 1618 UTC)”**

353

354 **Development and application of the WRFDA-Chem 3DVAR system:**
355 **aiming to improve air quality forecast and diagnose model deficiencies**

356

357 Wei Sun^{1,2}, Zhiquan Liu^{2*}, Dan Chen^{3*}, Pusheng Zhao¹, and Min Chen¹

358 ¹ National Space Science Center, Chinese Academy of Sciences, Beijing, 100190, China

359 ² National Center for Atmospheric Research, Boulder, CO, 80301, USA

360 ³ Institute of Urban Meteorology, China Meteorology Administration, Beijing, 100089, China

361

* Corresponding author: Dr. Zhiquan Liu (liuz@ucar.edu) and Dr. Dan Chen (dchen@ium.cn)

362 **Abstract**

363 To improve the operational air quality forecasting over China, a new aerosol/gas phase pollutants
364 assimilation capability is developed within the WRFDA system using 3DVAR algorithm. In this first
365 application, the interface for MOSAIC aerosol scheme is built with flexible extending potentials.
366 Based on the new WRFDA-Chem system, five experiments assimilating different surface observations,
367 including PM_{2.5}, PM₁₀, SO₂, NO₂, O₃, and CO are conducted for January 2017 along with a control
368 experiment without DA. Results exhibit that the WRFDA-Chem system evidently improves the air
369 quality forecasting. On the analysis aspect, the assimilation of surface observations reduces the bias
370 and RMSE in the initial condition (IC) remarkably; on the forecast aspect, better forecast performances
371 are acquired up to 24-h, in which the experiment assimilating the six pollutants simultaneously displays
372 the best forecast skill overall. With respect to the impact of DA cycling frequency, the responses
373 toward IC updating are found out to be different among the pollutants. For PM_{2.5}, PM₁₀, SO₂, and CO,
374 the forecast skills increase with the DA frequency. For O₃, although improvements are acquired at the
375 6-h cycling frequency, the advantage of more frequent DA could be consumed by the disadvantages
376 of the unbalanced photochemistry (due to inaccurate precursor NO_x/VOC ratios) or the changed
377 titration process (due to changed NO₂ concentrations but not NO) from assimilating the existing
378 observations (only O₃ and NO₂, but no VOC and NO); yet the finding is based on the 00 UTC forecast
379 for this winter season only and O₃ has strong diurnal and seasonal variations, more experiments should
380 be conducted to draw further conclusions. In addition, considering after one aspect (IC) in the model
381 is corrected by DA, the deficiencies from other aspects (e.g., chemical reactions) could be more evident,
382 this study explores the model deficiencies by investigating the effects of assimilating gaseous
383 precursors on the forecast of related aerosols. Results exhibit that the parameterization (uptake

删除的内容: forest
删除的内容: 2.5
删除的内容: 10
删除的内容: 2
删除的内容:
带格式的: 字体:小四
带格式的: 字体:小四
带格式的: 字体:小四
带格式的: 字体:Times, 小四, 非 粗体, 字体颜色: 自动
带格式的: 字体:Times, 小四, 非 粗体, 字体颜色: 自动
带格式的: 字体:Times, 小四, 非 粗体, 字体颜色: 自动
带格式的: 字体:Times, 小四, 非 粗体, 字体颜色: 自动
带格式的: 字体:Times, 小四, 非 粗体, 字体颜色: 自动
删除的内容: ; for O3, although improvements are acquired at the 6-h cycling frequency, the advantage of more frequent DA could be consumed by the disadvantage of unbalanced photochemistry (due to inaccurate precursor NO _x /VOC ratios) and changed titration process (due to changed NO ₂ concentrations but not NO) from assimilating the existing observations (only O ₃ and NO ₂ , but no VOC nor NO); but the finding is based on the 00 UTC forecast for this winter season only, due to the strong diurnal and seasonal changes of O ₃ , more experiments should be conducted to draw solid conclusions.
删除的内容: C
带格式的: 字体:小四
删除的内容: further

402 coefficients) in the newly added Sulfate-Nitrate-Ammonium (SNA) relevant heterogeneous reactions
403 in the model are not fully appropriate although it best simulates observed SNA aerosols without DA;
404 since the uptake coefficients were originally tuned under the inaccurate gaseous precursor scenarios
405 without DA, the biases from the two aspects (SNA reactions and IC DA) were just compensated. In
406 the future chemistry development, parameterizations (such as uptake coefficients) for different gaseous
407 precursor scenarios should be adjusted and verified with the help of DA technique. According to these
408 results, DA ameliorates certain aspects by using observation as constraints, and thus provides an
409 opportunity to identify and diagnose the model deficiencies; it is useful especially when the
410 uncertainties of various aspects are mixed up and the reaction paths are not clearly revealed. In the
411 future, besides being used to improve the forecast through updating IC, DA could be treated as another
412 approach to explore necessary developments in the model.

413 1. Introduction

414 Air pollution is almost inevitable for all developed (historically) and developing (in present days)
415 countries. From acid rain, haze to smog etc., the air pollution significantly impacts atmospheric
416 visibility, human health, and climate. As one of the fastest-growing countries, China has been suffering
417 from the extreme haze with high particulate matter (PM) national-wide and increasing tropospheric
418 ozone (O₃) pollution in city clusters (Fu et al., 2019; Lu et al., 2019). To control the pollutions as well
419 as to improve the air quality forecast, Chinese governments had enforced stricter air quality standards
420 from 2012, and deployed monitoring network for six “criteria” air pollutants since 2013, which
421 includes PM_{2.5} and PM₁₀ (aerosols/fine particulate matter with aerodynamic diameters less than 2.5 or
422 10 μm), SO₂ (sulfur dioxide), NO₂ (nitrogen dioxide), O₃ (ozone), and CO (carbon monoxide). Among

删除的内容:

424 the six pollutants, the forecast on aerosols (especially PM_{2.5}) is of greatest research interest as the
425 severity of aerosol pollution and its negative effects on both health and climate. However, it's still
426 challenging to accurately simulate and forecast aerosols by pure air quality models due to some issues,
427 such as the large uncertainties in primary and precursor emissions processes, the incomplete
428 understanding and parameterization of secondary inorganic/organic reactions from precursors, and the
429 accumulation of meteorology simulation errors. In addition to aerosol forecast, the elevated O₃ levels
430 in city clusters over eastern China draw more and more attentions recently. Under this circumstance,
431 in the urban regions in China, where suffer from complex air pollution with both haze and smog, the
432 accurate forecast of air quality has been not only a challenge for operational centers, but also a common
433 concern for [the](#) scientific community.

434 To improve the forecast skill, data assimilation (DA), a combination of observations and numerical
435 model output, has been widely used in meteorology forecast since last century, and recently extended
436 to air pollutant forecasts. Based upon various techniques, DA is proven to be skillful at improving the
437 meteorology and aerosol forecasts (Bannister 2017; McHenry et al. 2015; Peng et al. 2018; Sandu and
438 Chai 2011; Schutgens et al. 2010; Sekiyama et al. 2010; Tang et al. 2011; Tang et al. 2013). Focusing
439 on aerosol assimilation, NCAR group had conducted a series of work. Using three-dimensional
440 variational (3DVAR) algorithm, Liu et al. (2011) implemented DA on aerosol optical depth estimates
441 within the Grid-point Statistical Interpolation (GSI) system. Schwartz et al. (2012), Jiang et al. (2013),
442 and Chen et al. (2019) further extended this system to assimilate surface PM_{2.5} and PM₁₀. It should be
443 noted that the aerosols are complicated not merely from primary emissions but also secondary
444 reactions with gaseous precursors in the atmosphere (Huang et al. 2014; Nie et al. 2014; Xie et al.
445 2015). However, the assimilation of aerosols along with gas phase pollutants are seldom investigated.

446 Recently, it is encouraging that an Ensemble Kalman Filter (EnKF) DA system is developed to
447 assimilate multi-species surface chemical observations (Peng et al. 2017), while the EnKF system may
448 not be the favorite choice in operational applications due to its massive computational cost. In addition,
449 at the Institute of Urban Meteorology (IUM), regional NWP system–RMAPS-ST (adapted from WRF)
450 and regional air quality model–RMAPS-Chem (adapted from WRF-Chem) are applied operationally
451 for the weather and air quality forecast over Northern China. RMAPS-ST provides the meteorology
452 drivers for RMAPS-Chem, and WRFDA is utilized for the meteorology DA in RMAPS-ST (Fan et al.
453 2016; Yu et al. 2018). In result, to implement the assimilations of aerosols along with gas phase
454 pollutants in the future air quality forecast operational system (e.g. the RMPAS-Chem), and to design
455 an efficient and unified DA platform that satisfies the operational needs in both meteorology and air
456 quality forecast, this study works on the WRFDA system with 3DVAR algorithm. To the authors’
457 knowledge, this is the first attempt to assimilate hourly ground-based aerosols simultaneously with gas
458 phase pollutants in the WRFDA system.

459 With regard to the aerosol data assimilation, the first and foremost challenge comes from the
460 complex components related to the aerosol scheme. With different emphasis and applications, the
461 chosen aerosol scheme in the model could be different, which will lead to various choices and
462 treatments for the analysis variables in the DA system. For example, in the existed DA developments,
463 many studies used the GOCART aerosol scheme to address the dust or the natural-source related events.
464 However, the GOCART aerosol scheme is well known to underestimate the PM concentrations due to
465 lack of secondary organic aerosol (SOA) formation, as well as aerosol species related to the
466 anthropogenic emission, such as nitrate and ammonium (McKeen et al. 2009; Pang et al. 2018).
467 Different from the GOCART scheme, the MOSAIC (Model for Simulating Aerosol Interactions and

468 Chemistry) aerosol scheme uses a sectional approach to represent the aerosol size distribution with
469 different size bins, and it takes black carbon, organic carbon, sulfate, nitrate, ammonium, sodium,
470 chloride, and other inorganic compounds that are related to anthropogenic emissions into consideration.
471 In result, the MOSAIC scheme exhibits a better performance in representing the complex PM_{2.5}
472 pollution over China (Chen et al. 2016; Chen et al. 2019). Therefore, to make the DA system suitable
473 for different emphasis and applications, a flexible aerosol assimilation capability is built within the
474 WRFDA system in this study, which will facilitate developments and applications for more chemistry
475 schemes in the future. Focusing on the air quality forecast over China, this study mainly analyses the
476 results of MOSAIC aerosol scheme.

477 It should be mentioned that the forecast performance with DA also relies on the air quality model
478 itself. Due to the limited observational information as constraint, the DA system uses large parts of
479 model mechanism and processes to derive the full analysis information (e.g. use total PM mass
480 observations to analyze all PM components). However, there are still potential deficiencies in the
481 model. For example, some reaction paths are missing in the heavily polluted events in China (e.g.
482 Wang et al., 2014), since the chemistry schemes are originally developed for relatively clean areas and
483 recently observed pathways haven't been timely reflected in the model. Moreover, the large
484 uncertainties of precursor and primary emissions could bring errors to the aerosol species partitioning
485 and size distribution in the model. Nevertheless, when it comes to DA, as one aspect (initial conditions
486 of aerosols and some precursors) in the model is corrected by using observation as constraints, the
487 deficiencies from other aspects, such as the above mentioned chemical reactions, could be more
488 evident. From this point of view, after investigating to what extent the DA technique can help to

删除的内容: data assimilation

删除的内容: d

491 improve the forecast of air quality, this study further explores the model deficiencies with the help of
492 DA, aiming to provide helpful indications for future model development.

493 In the rest of the paper, an overview of the model description, observations, and methodology is
494 presented in Section 2, followed by evaluations of the new WRFDA-Chem system in Section 3.
495 Section 4 analyzes the DA experiments in consideration of potential issues in the model, aiming to
496 provide beneficial references on further model development. Conclusions and discussions are given in
497 section 5.

498 **2. Model description, observations, and methodology**

499 In this study, the interfaced air quality model is WRF-Chem. The WRF-Chem settings are very
500 similar to those of Chen et al. (2016). Here, only a summary of the model configuration and
501 observations is provided below. Descriptions of the most important development of this study, the
502 WRFDA-Chem system, are presented in Section 2.3.

503 **2.1 WRF-Chem model and emissions**

504 As in Chen et al. (2016), version 3.6.1 of the WRF-Chem model is used in this study to simulate
505 the aerosols and gas-phase chemistry processes. A summary of the used physical parameterizations is
506 given in Table 1. Details of the WRF-Chem model have been described by Grell et al. (2005) and Fast
507 et al. (2006). The Carbon Bond Mechanism version Z (CBMZ) and Model for Simulating Aerosol
508 Interactions and Chemistry (MOSAIC) schemes are used as the gas-phase and aerosol chemical
509 mechanisms, respectively. The relative humidity (RH) dependent heterogeneous reactions added by
510 Chen et al. (2016) are also applied in the simulations. The model computational domain covers most

删除的内容: brief

512 of China and its surrounding regions. Figure 1 presents the horizontal range of the domain, which
513 contains 121 x 121 horizontal grids at a 40.5-km resolution. Vertically, there are 57 levels extending
514 from the surface to 10 hPa.

515 As in Chen et al. (2019), the emission input is based on the 2010 Multi-resolution Emission
516 Inventory for China (MEIC) (He 2012; Lei et al. 2011; Li et al. 2014; Zhang et al. 2009), which has
517 already been applied in many recent studies over China (Wang et al. 2016; Wang et al. 2013; Zheng
518 et al. 2015). The emission inventory has also been processed to match the model grid spacing (40.5
519 km) from an original grid spacing of $0.25^\circ \times 0.25^\circ$ (Chen et al. 2016). Admittedly, the difference
520 between the emission base year and our simulation year and the spatial-temporal allocations may arise
521 uncertainties in our simulation, this emission is the only publicly available emission inventory when
522 the study is conducted. Meanwhile, the inhomogeneous spatial changes and large uncertainties in
523 seasonal allocations of the emissions made it difficult to simply scale the original emission inventory
524 for our study period (Chen et al. 2019).

525 The dust emission is the GOCART dust emission and the biogenic emission is calculated online
526 by the Gunther scheme within the WRF-Chem model. Given the time period of this study (January) is
527 not the period with massive fires (crop/biomass burning), the fire emission is not used in this study.

带格式的: 字体:Times, 小四, 非 粗体

528 2.2 Observations

529 For the future application in RMAPS-Chem operational air quality forecast system, the WRFDA-
530 Chem system is designed to assimilate the hourly surface observations of six major pollutants (PM_{2.5},
531 PM₁₀, SO₂, NO₂, O₃, and CO) from the China National Environmental Monitoring Center (CNEMC).
532 To verify the capability of the system, we use the data for the whole month of January 2017. As in

533 Chen et al. (2019), to perform statistical calculations, an observation dataset at 531 locations (Fig. 1)
534 is acquired by averaging all the original observations (1600+ sites) that fall into the same model grid.
535 Meanwhile, two steps of data quality control are conducted before DA. Firstly, observations larger than
536 a threshold are treated as unrealistic and are not assimilated. Secondly, observations leading to
537 innovations (observations minus the model-simulated values) higher than a maximum deviation are
538 omitted. For PM_{2.5}, PM₁₀, SO₂, NO₂, O₃, and CO, the threshold in the first step is 500 μg m⁻³, 700 μg
539 m⁻³, 200 μg m⁻³, 200 μg m⁻³, 200 μg m⁻³, and 20 mg m⁻³, respectively; the maximum deviation in the
540 second step is 120 μg m⁻³, 120 μg m⁻³, 60 μg m⁻³, 60 μg m⁻³, 60 μg m⁻³, and 6 mg m⁻³, respectively.

541 To verify sulfate-nitrate-ammonium partitioning, a site observation of different chemical species
542 is used in Section 4. The measurements were performed over January 14–20, 2017, and carried out on
543 the roof of IUM in Beijing (green dot in Fig. 1). A detailed description for the features of the
544 observation, including the quality assurance and quality control has been given by Su et al. (2018).
545 This study mainly uses the sulfate (SO₄²⁻) and nitrate (NO₃⁻) in this dataset.

546 2.3 WRFDA-Chem system

547 In this study, an aerosol/chemical assimilation capability is built within the version 4.0.3 of the
548 WRFDA system with 3DVAR algorithm. The WRFDA 3DVAR produces the analysis through the
549 minimization of a scalar objective function $J(x)$ given by

$$550 \quad J(x) = \frac{1}{2}(x - x_b)^T B^{-1}(x - x_b) + \frac{1}{2}[H(x) - y]^T R^{-1}[H(x) - y], \quad (1)$$

551 where x_b denotes the background vector, y is a vector of the observations, and B and R
552 represent the background and observation error covariance matrices, respectively. The covariance
553 matrices determine how close the analysis is weighted toward the background and observations. H is

带格式的: 正文, 缩进: 首行缩进: 0.63 cm

554 the observation operator that interpolates model grid point values to observation space and converts
555 model-predicted variables to observed quantities.

带格式的

556 Generally, the implementation of WRFDA-Chem 3DVAR includes several parts: WRF-Chem
557 model and surface air pollutants observation interface to WRFDA, the addition of aerosol/chemical
558 analysis variables, the surface air pollutants observation operators, the update of observation errors,
559 and the statistics of background error covariances for chemical analysis variables. Detailed
560 descriptions will be presented in the following parts. It's worth mentioning that the new WRFDA-
561 Chem system is designed with a flexible aerosol assimilation capability that can switch between
562 different aerosol schemes. Given the fact that WRF-Chem model predicts the PM concentrations in
563 the forms of different prognostic variables depending on the chosen aerosol scheme, the
564 aerosol/chemical prognostic variables are given in the registry file of the WRFDA-Chem, instead of
565 specifically defined in the code. With the help of the registry mechanism of WRF model, the prognostic
566 variables in the entire DA process can be easily adjusted by modifying the registry file. The WRFDA-
567 Chem system has been tested with GOCART and MOSAIC aerosol scheme, while this study focuses
568 on the MOSAIC scheme.

569 2.3.1 Observation operators

570 The WRFDA-Chem is designed to assimilate six types of surface aerosol/chemical observations,
571 including PM_{2.5}, PM₁₀, SO₂, NO₂, O₃, and CO. For aerosol assimilation, the aerosol species in the
572 MOSAIC scheme are defined as black carbon (BC), organic compounds (OCs), sulfate (SO₄²⁻), nitrate
573 (NO₃⁻), ammonium (NH₄⁺), sodium (NA), chloride (CL), and other inorganic compounds (OIN). To
574 represent the aerosol size distribution, MOSAIC uses a sectional approach with different bins. This

575 study uses four size bins with aerosol diameters ranging from 0.039–0.1, 0.1–1.0, 1.0–2.5, and 2.5–
576 10 μ m. The PM_{2.5} total is controlled by the 24 variables in the first three bins (8 species multiplied by
577 3 bins), and the PM₁₀ total is controlled by the 32 variables in the four bins (8 species multiplied by 4
578 bins). In result, the model-simulated PM_{2.5} is computed by summing the 24 variables as

$$579 \quad y_{PM_{2.5}}^f = \rho_d \sum_{i=1}^3 [BC_i + OC_i + SO_{4i} + NO_{3i} + NH_{4i} + CL_i + NA_i + OIN_i]. \quad (2)$$

580 The model-simulated PM₁₀ observations are computed by summing the 32 variables as

$$581 \quad y_{PM_{10}}^f = \rho_d \sum_{i=1}^4 [BC_i + OC_i + SO_{4i} + NO_{3i} + NH_{4i} + CL_i + NA_i + OIN_i]. \quad (3)$$

582 Correspondingly,

$$583 \quad y_{PM_{10-2.5}}^f = \rho_d \sum_{i=4}^4 [BC_i + OC_i + SO_{4i} + NO_{3i} + NH_{4i} + CL_i + NA_i + OIN_i], \quad (4)$$

584 where ρ_d is the dry-air density, which is used to convert the unit of the analysis variable (μ g/kg) to
585 the observations (μ g/m³); i denotes the bin number in the MOSAIC aerosol scheme. In the
586 experiment assimilating PM_{2.5} alone, the PM_{2.5} observations are used to analyze the species in the first
587 three bins (Eq. 2). In the experiment assimilating PM_{2.5} and PM₁₀ simultaneously, the PM_{2.5}
588 observations are used to analyze the species in the first three bins (Eq. 2), and the PM_{10-2.5} (PMcoarse,
589 hereafter) in the observations is used to analyze the species in the 4th bin (Eq. 4). A similar approach
590 has been adopted by Peng et al. (2018).

591 In the assimilation of the gas-phase pollutants, the model-simulated values are computed by

$$592 \quad y_x^f = \rho_d \cdot \frac{M_x}{M_{dair}} \cdot R_x \cdot 10^3, \quad (5)$$

593 where x denotes the four gas-phases pollutants as in SO₂, NO₂, O₃, and CO, ρ_d is the dry-air density,
594 M_x is the relative molecular mass for the four gas-phases pollutants, M_{dair} is the relative molecular
595 mass for dry-air, and R_x is the mixing ratio for the four gas-phases pollutants. Since the gas-phase

删除的内容: are

597 pollutants observations are mass concentrations in $\mu\text{g}/\text{m}^3$ and the analysis variables are mixing ratios
598 in ppmv, the Eq. 5 is used for the unit conversion.

599 2.3.2 Observation errors

600 Following Chen et al. (2019) and Peng et al. (2018), the observation error covariance matrix \mathbf{R} in
601 Eq. (1) is estimated from measurement error ε_0 and the representativeness error ε_r in this study. The
602 measurement error ε_0 is defined as $\varepsilon_0 = 1.0 + 0.0075 \cdot M_i$, where M_i denotes the observation of
603 the six major pollutants in unit $\mu\text{g}/\text{m}^3$; the representativeness error ε_r is defined as $\varepsilon_r = \gamma \varepsilon_0 \sqrt{\frac{\Delta x}{L}}$,
604 where γ is an adjustable parameter scaling (set as 0.5), Δx is the grid spacing (40.5 km in our case)
605 and L is the radius of influence of the observation (set to 2 km). These parameter settings are based
606 on the sensitivity tests by Chen et al. (2019). The total observation error (ε_x) is computed as $\varepsilon_x =$
607 $\sqrt{\varepsilon_{0x}^2 + \varepsilon_{rx}^2}$, where x denotes the six major pollutants as in PM_{2.5}, PM₁₀, SO₂, NO₂, O₃, and CO.

608 2.3.3 Background error covariance

609 To implement the aerosol/chemical DA with the MOSAIC-4Bin scheme, this study expands the
610 GEN_BE v2.0 (Descombes et al. 2015) to compute the \mathbf{B} matrix in Eq. (1) for the 32 chemical variables
611 as in Eq. 3 (BC, OC, SO₄²⁻, NO₃⁻, NH₄⁺, NA, CL, and OIN in four bins), as well as the four gas-phase
612 variables as in Eq. 5 (SO₂, NO₂, O₃, and CO). Since it is both technically and scientifically challenging
613 to model the cross-correlations between different aerosol/chemical variables in a 3DVAR framework,
614 they are not considered in this study. We plan to introduce the cross-variable correlations with the
615 ensemble-variational approach in the future extension of the system. With the updated GEN_BE v2.0,

删除的内容: Cross-correlations between different aerosol/chemical variables were not considered.

带格式的: 字体:Times, 小四, 非 粗体

带格式的: 字体:Times, 小四, 非 粗体

618 the statistics for background error covariance, such as standard deviation, vertical and horizontal length
619 scales, and vertical correlations, are computed for each of the aerosol/chemical variables. In this study,
620 the background error covariance is estimated using the National Meteorological Center (NMC) method
621 (Parrish and Derber, 1992) from one-month WRF-Chem forecasts over January 2017.

622 Following the analyses based on the GEN_BE v2.0 (Descombes et al. 2015), Figure 2 presents the
623 background error standard deviations of each species at different vertical levels. For the aerosols in the
624 first three size bins (Fig. 2a-2c), although the standard deviation errors vary across the species, the
625 errors of NO_3^- , SO_4^{2-} , NH_4^+ , OC, and OIN are generally larger than that of the others (BC, CI and NA)
626 in the three size bins. These results are consistent with the finding in Chen et al. (2019), which allows
627 inorganic compounds (NO_3^- , SO_4^{2-} , NH_4^+), OC and OIN to be adjusted more in corresponding to their
628 larger background errors. For the aerosols in the 4th size bin (Fig. 2d), the errors are unreasonably
629 much smaller than that in the first three bins due to model deficiency. Under this circumstance, to get
630 a reasonable bigger adjustment for the aerosols in the 4th size bin, it might need to enlarge their
631 background errors in the DA procedure. As for the gaseous pollutants (Fig. 2e), CO has the biggest
632 background errors in the middle and lower layers, followed by O_3 , SO_2 and NO_2 .

633 For the background error horizontal correlation length scales, the results are similar as in Liu et al.
634 (2011) (figure omitted). The length scales of aerosols are comparable in most of the species, which
635 generally span from 1.5 to 2.5 times the grid spacing, while the aerosol species NA exhibits a smaller
636 horizontal length scale than all the other species. For the background error vertical correlations (figure
637 omitted), the results are similar as in Descombes et al. (2015), in which the vertical correlations are
638 bigger in the lower levels (where they are emitted) in most of the species. According to Descombes et

带格式的: 字体:Times, 小四, 非 粗体
带格式的: 缩进: 首行缩进: 0.63 cm

带格式的: 字体:小四
带格式的: 字体:小四
带格式的: 字体:小四
带格式的: 字体:Times, 小四, 非 粗体
带格式的: 字体:小四
带格式的: 字体:小四
带格式的: 字体:Times, 小四, 非 粗体
带格式的: 字体:小四
带格式的: 字体:小四
带格式的: 字体:小四
带格式的: 字体:Times, 小四, 非 粗体
带格式的: 字体:Times, 小四, 非 粗体
带格式的: 字体:小四
带格式的: 字体:小四
带格式的: 字体:Times, 小四, 非 粗体
带格式的: 字体:小四
带格式的: 字体:Times, 小四, 非 粗体
带格式的: 字体:Times, 小四, 非 粗体
带格式的: 字体:小四
带格式的: 字体:Times, 小四, 非 粗体
带格式的: 字体:Times, 小四, 非 粗体
带格式的: 字体:六号
带格式的: 字体:六号
带格式的: 字体:Times, 小四, 非 粗体
带格式的: 字体:Times, 小四, 非 粗体
带格式的: 字体:Times, 小四, 非 粗体

639 al. (2015), the reactions with species emitted near the surface might create these strong correlations in
640 the lower model levels.

带格式的: 字体:Times, 小四, 非 粗体

641 2.3.4 Experimental design

642 To seek for the best forecast performance, six experiments were conducted for January 2017 in
643 this study, including NODA, PM1, PM2, ALL, ALL_3h, and ALL_1h (detailed in Table 2). NODA is
644 the control experiment without any data assimilation. The design of PM1, PM2, and ALL is to
645 investigate the assimilation impacts of PM_{2.5}, PMcoarse, and gas-phase pollutants (SO₂, NO₂, O₃, CO)
646 step-by-step.

647 The NODA experiment initialized a new WRF-Chem forecast every 6-h between 00:00 UTC, 20
648 December 2016 and 18:00 UTC 31 January 2017, in which the aerosol/chemical fields were simply
649 carried over from cycle to cycle, and the meteorological initial condition/boundary conditions were
650 updated from GFS data every 6-h. The first 10 days were treated as the spin up period, and only
651 simulations in January were used in the following analyses. The PM1, PM2, and ALL experiments
652 updated the chemical IC using the WRFDA-Chem system every 6-h starting from 00:00 UTC, 1
653 January. The background of the first cycle was obtained from the NODA experiment, and all
654 subsequent cycles were derived from the 6-h forecast of the previous cycle. The only difference
655 between PM1, PM2, and ALL experiments is that PM1 only assimilated PM_{2.5} observations; PM2
656 assimilated PM_{2.5} and PMcoarse (PM_{10-2.5}) simultaneously; ALL assimilated PM_{2.5}, PM_{10-2.5},
657 SO₂, NO₂, O₃, and CO together.

带格式的: 缩进: 首行缩进: 0.63 cm, 定义网格后自动调整右缩进, 空格 段后: 0 磅, 调整中文与西文文字的间距, 调整中文与数字的间距

带格式的: 字体颜色: 自动
带格式的: 字体:小四
带格式的: 字体:小四
带格式的: 字体:小四
带格式的: 字体:小四
带格式的: 字体:小四
带格式的: 字体颜色: 自动

658 In view of the cycling frequency is an important aspect in the DA strategy, especially for 3DVAR,
659 two more experiments that assimilate all the six major pollutants with 3-h and 1-h cycling frequency
660 are conducted respectively (experiment ALL 3h and ALL 1h). To investigate the forecast
661 improvements, a 24-h forecast is initialized for all the experiments at 00:00 UTC of each day.

带格式的: 字体:Times, 小四, 非 粗体

删除的内容: In view of the cycling frequency is an important aspect in the DA strategy, especially for 3DVAR, two more experiments assimilating all the six major pollutants with different cycling frequencies are further conducted, in which the ALL_3h and ALL_1h experiments assimilate the data with 3-h and 1-h cycling frequency, respectively.

662 3. Performance of the WRFDA-Chem system

663 3.1 Impact on analyses

664 To evaluate the performance of the WRFDA-Chem system, the impact on analyses is firstly
665 investigated. Figure 3 presents the domain-averaged bias and root-mean-square-error (RMSE) of the
666 analysis at 00 UTC over January 1-31, 2017. For PM_{2.5} (Fig. 3a), the NODA experiment displays a
667 general overestimation of 36.60 μg/m³, along with a large RMSE of 70.41 μg/m³. After DA, in the
668 PM1, PM2, and ALL experiments, the bias of PM_{2.5} drops to 5.62 μg/m³, 5.19 μg/m³, and 5.98 μg/m³,
669 respectively; the RMSE drops to 22.10 μg/m³, 22.84 μg/m³, and 23.15 μg/m³, respectively.

删除的内容: 2

删除的内容: 2

删除的内容: .

670 In the analyses of PM₁₀, it is noted that the PM1 experiment has a larger bias than the NODA run
671 (Fig. 3b). To explain this phenomenon, Figure 4 presents the monthly mean difference between PM₁₀
672 and PM_{2.5} (PM₁₀ minus PM_{2.5}, PMcoarse) in the analysis. In the observation, the PMcoarse generally
673 increases from south to north, reaching above 50 μg/m³ over northern China (Fig. 4a). However, the
674 PMcoarse in the NODA experiment (with an average of 5.47 μg/m³) is much smaller than that in the
675 observation (with an average of 39.13 μg/m³). This result suggests that the WRF-Chem model failed
676 to reasonably represent the PMcoarse, which is actually the 4th bin of the aerosol species in the
677 MOSAIC scheme. Under this circumstance, when the assimilation of PM_{2.5} trying to reduce its evident
678 overestimation (Fig. 3a), components in the first three bins (within 2.5 μm) of PM₁₀ decrease

删除的内容: 2

删除的内容: 3

删除的内容: 3

删除的内容: 2

692 dramatically. Meanwhile, since the simulated PMcoarse is too small, the PM₁₀ variates are eventually
693 dominated by the adjustment of PM_{2.5}. In result, the assimilation of PM_{2.5} causes a large negative bias
694 in the PM₁₀ analysis (Fig. 3b). Correspondingly, compared to the NODA run, the PMcoarse in the PM1
695 experiment exhibit no significant changes (only slightly decrease) in the analysis (Figs. 4b and 4c) and
696 also in the forecast (Fig 4f).

697 To overcome this issue, several adjustments have been adapted in the PM₁₀ assimilation: instead
698 of using the PM₁₀ observations directly, the PMcoarse is used to analyze the species in the 4⁺ bin (Eq.
699 4); to reflect the large uncertainty of the simulated PMcoarse and to appropriately weighting the model
700 and observation errors, the background error covariance of the PMcoarse (species in the 4⁺ bin) is
701 arbitrarily inflated (inflation factor 1 is normally used and 90 is selected after tuning). By this means,
702 after assimilating the PM₁₀ observations, the PM2 and ALL experiments exhibit similar distributions
703 in the PMcoarse (Figs. 4d-e, with an average of 34.58 μg/m³ and 34.68 μg/m³) as in the observation
704 (with an average of 39.13 μg/m³). Correspondingly, compared to the NODA experiment, evident
705 improvements for PM₁₀ analysis appear in the PM2 and ALL experiments, in which the bias and RMSE
706 drops evidently (Fig. 3b). Overall, the DA experiments exhibit strong contributions to the analyses of
707 PM_{2.5} and PM₁₀, suggesting that the WRFDA-Chem system works effectively in updating the initial
708 conditions.

709 As for the analyses of gaseous pollutants (Figs. 3c-3f), large improvements can be seen in the ALL
710 experiment by further assimilating SO₂, NO₂, O₃, and CO. Compared to the PM2 experiment, although
711 the bias and RMSE for PM_{2.5} and PM₁₀ in the ALL experiment are slightly larger, the bias for the four
712 gaseous pollutants decrease from 4.74 μg/m³, -4.59 μg/m³, 4.92 μg/m³, and -8.31 mg/m³ (PM2
713 experiment) to -1.68 μg/m³, -1.25 μg/m³, -0.31 μg/m³, and -0.18 mg/m³ (ALL experiment),

删除的内容: 2

删除的内容: 3

删除的内容: 3

删除的内容: 3

删除的内容: 3

删除的内容: 2

删除的内容: .

删除的内容: 2

删除的内容: 2

删除的内容: is

724 respectively, and the corresponding RMSE drops from $37.87 \mu\text{g}/\text{m}^3$, $15.39 \mu\text{g}/\text{m}^3$, $21.04 \mu\text{g}/\text{m}^3$, and
725 $1.11 \text{ mg}/\text{m}^3$ (PM2 experiment) to $23.85 \mu\text{g}/\text{m}^3$, $9.70 \mu\text{g}/\text{m}^3$, $8.62 \mu\text{g}/\text{m}^3$, and $0.43 \text{ mg}/\text{m}^3$ (ALL
726 experiment). In general, by assimilating all the six major pollutants, the ALL experiment displays the
727 largest improvement in the analyses of gaseous pollutants among all the experiments, along with a
728 comparable improvement in the analyses of the aerosols.

729 Due to the lack of vertical information within the observations, the common mathematical solution
730 to use the surface total mass observations to analyze multiple 3-D fields variables is to utilize prior
731 information in the background. As shown in Fig. 5, based on vertical correlations specified in the
732 background error covariance, the observation impact spreads to a certain height, even though the
733 analysis variables used in the observation operator (Eq. 2-5) are only at the lowest model level. It is
734 also noted that observations contribute differently to the analysis variables. Corresponding to the
735 strong overestimation of PM_{2.5} (Fig. 3a), all the three DA experiments (PM1, PM2 and ALL) tend to
736 reduce the PM_{2.5} below 6 km; corresponding to the distinct underestimation for CO (Fig. 3f), the
737 experiment assimilating CO (ALL experiment) increases the value below 9 km. Relative small analysis
738 increments are shown in the other three gas pollutants (SO₂, NO₂, and O₃).

739 3.2 Forecast improvements

740 After illustrating the effect of WRFDA-Chem on the analyses, this section further investigates the
741 forecast performances based on the new analyses. A 24-h forecast is performed at each 00 UTC from
742 1 to 31 January 2017. The forecast error statistics, including bias, RMSE, and correlation, are computed
743 by verifying against the surface observations at 531 stations over China.

删除的内容: 4

删除的内容: among

删除的内容: 2

删除的内容: 2

748 As shown in Fig. 6, the model performs relative poorly in the forecast of aerosols without DA.
749 For PM_{2.5}, the average bias, RMSE, and correlation over 0-24 h are 31.17 μg/m³, 88.99 μg/m³, and
750 0.41, respectively (Tab. 3). As expected, all the DA experiments improve the forecasts evidently.
751 Along with the forecast range, distinct improvements on bias, RMSE and correlation last from 0 to 24
752 h. For example, in PM1 experiment, the average improvement percentages (over 0-24 h) for bias,
753 RMSE and correlation reach up to 71.8%, 39.4%, and 43.9%, respectively. It is also noted that PM_{2.5}
754 observation is the dominant data source in improving PM_{2.5} forecast. As for PM₁₀, distinct
755 improvements on RMSE and correlation can be seen from 0 to 24 h. Especially after assimilating the
756 PMcoarse (PM_{10-2.5} in PM2 and All experiments), the averaged improvement percentage for RMSE
757 and correlation reach up to about 27.0% and 55.5%. For bias, since the statistics are averaged over the
758 531 stations, the offset of large positive and negative bias at different stations leads to the small
759 averaged bias in the NODA run (see the spatial distribution of bias at the individual site in Section 1
760 of the supplementary material). Considering the DA experiments exhibit distinct improvements on
761 RMSE and correlation, WRFDA-Chem still provides a generally positive contribution to the PM₁₀
762 forecast.

763 Figure 7 presents the averaged forecast error statistics for SO₂, NO₂, O₃, and CO with respect to
764 forecast range. In PM1 and PM2 experiments that do not assimilate the gas-phase observations, no
765 significant changes appear in the forecasts of the gaseous pollutants compared to the NODA run; after
766 assimilating the gas-phase observations, the ALL experiment shows evident improvements in all the
767 four gaseous pollutants, in which the improvements for SO₂, NO₂, and O₃ are more significant in 0-10
768 h, and the improvements for CO last up to 24 h. According to the numbers shown in Table 3, for SO₂,
769 NO₂, O₃, and CO, the average bias (RMSE) in the ALL experiment decreases by 43.3%, 42.2%, 73.9%,

删除的内容: 5

删除的内容: ly

删除的内容: Averaging over 0-24 h, the

删除的内容: 2.4

删除的内容: 0

删除的内容: 6

删除的内容: 2

删除的内容: 6

删除的内容: 13.4

删除的内容: 3

删除的内容: 4

删除的内容: 0

782 and 74.0% (13.4%, 5.3%, 11.3%, and 33.7%), compared to the NODA run, and the average correlation
783 increases by 37.9%, 8.3%, 41.4%, and 103.5%, respectively. It is worth noting that the WRFDA-Chem
784 system has a positive impact on the forecast of NO₂ and O₃ by merely analyzing the IC. Since NO₂
785 and O₃ are related to complex photochemical reaction processes, the assimilation of NO₂ and O₃
786 usually does not work well as other gas-phase pollutants on the forecast aspect, even with both
787 emission and IC analyzed (Peng et al. 2018). In result, the aerosol/chemical assimilation based on
788 WRFDA-Chem could not only contribute to the conventional aerosol forecasts in operational
789 applications, but also provide valuable help in the emerging study demands for gaseous pollutants,
790 especially O₃.

791 Air Quality Index (AQI), which is used for reporting daily air quality and issuing alarms, is one
792 of the service products of RMAPS-Chem operational air quality model over Northern China. Generally,
793 AQI is classified into six levels rating from good to hazardous: 0-50 (level 1), 51-100 (level 2), 101-
794 150 (level 3), 151-200 (level 4), 201-300 (level 5), and 300+ (Level 6). Similar to previous studies
795 (Kumar and Goyal 2011; Tao et al. 2015; Zheng et al. 2014), AQI is calculated for the six major
796 pollutants. The pollutant with the highest AQI level is deemed as the “main pollutant” and its AQI
797 determines the overall AQI level. Accordingly, the accurate forecast of AQI requires the overall good
798 performances of the six pollutants. To reflect the integrated DA effect of aerosols and gas-phase
799 pollutants, the threat score (TS), one of the most commonly used criteria in the verifications of
800 meteorology forecast, is used for AQI at each AQI level. The threat score (TS) for air quality index
801 (AQI) is calculated by

$$802 \quad TS_i = \frac{H_i}{H_i + M_i + F_i} \quad (6)$$

删除的内容: 5

删除的内容: 4

删除的内容: 8

删除的内容: 9

删除的内容: 6

删除的内容: 0

删除的内容: 0

删除的内容: ,

811 where H, M, and F denotes the times of the hits, the misses, and the false alarms in the forecast of
812 AQI, and i denotes the AQI levels from 1 to 6. In result, the TS is acquired at each AQI level ranging
813 from 0 to 1, and the higher (lower) TS represents the better (worse) forecast performance.

带格式的: 左对齐, 缩进: 首行缩进: 0 cm

814 As shown in Fig. 8, in the beginning of the forecast, DA experiments (PM1, PM2 and ALL)
815 increase the TS remarkably at all AQI levels, and then gradually decrease (quickly drop) with the
816 forecast range at AQI levels 2-6 (AQI level 1). Nevertheless, for the polluted situations with AQI levels
817 3-6, evident improvements can be seen from 0 to 24h in all the DA experiments, in which the average
818 TS increase from 0.19, 0.09, 0.16, and 0.19 (NODA experiment) to about 0.27, 0.16, 0.27, and 0.26
819 (DA experiments), respectively. For heavily polluted situations with AQI levels 5-6 (Figs. 8e-f),
820 compared to the PM1 case, TS experiences a further increase in the PM2 and ALL experiments after
821 assimilating the PMcoarse (PM_{10-2.5}). This result indicates that for heavily polluted events during this
822 period (January 2017), PM_{2.5} and PM₁₀ could be the “main pollutant” that contributes the most to the
823 AQI.

删除的内容: To reflect the integrated DA effect of aerosols and gas-phase pollutants, the threat score (TS, calculation methodology in Section 2 of the supplemental material) for AQI at each AQI level is further analyzed.

删除的内容: 7

删除的内容: y

删除的内容: 7

824 In general, the new WRFDA-Chem evidently improves the aerosol/chemical forecasting. Based
825 on the assimilation of the six major pollutants, the chemical ICs are improved distinctly and a better
826 forecast performance is acquired up to 24 hours. Among different experiments, the ALL experiment
827 displays the best forecast error statistics for most of the major pollutants along with the highest TS for
828 AQI. In the following operational applications, it is recommended to assimilate the six major pollutants
829 simultaneously, which will help to get better analyses and forecast skills on the whole.

837 3.3 Response to DA cycling frequency

838 Cycling frequency is an important aspect in the DA strategy. However, the responses toward IC
839 updating could be different among the pollutants. To figure out this issue and to provide helpful
840 references for future applications, DA experiments with different cycling frequencies were analyzed
841 in this section.

842 Figure 9 shows the domain-averaged bias and RMSE of the analysis as in Fig. 3, but for
843 experiments with different DA frequencies (ALL_6h, ALL_3h, and ALL_1h; ~~the ALL_6h is the ALL~~
844 ~~experiment in Tab.2~~). Except for O₃, most of the variables display a gradual improvement with the
845 increase of cycling frequency. For example, from NODA run to the 6-h cycling experiment, and then
846 to the 3-h and 1-h cycling experiment, the bias (RMSE) for PM_{2.5} gradually decrease from 36.60 μg/m³
847 (70.41 μg/m³) to 5.98 μg/m³ (23.15 μg/m³), and then to 5.41 μg/m³ (21.32 μg/m³) and 4.30 μg/m³
848 (18.54 μg/m³). Similar results also exist in the bias for SO₂, NO₂, and CO, as well as the RMSE for
849 PM₁₀, SO₂, and CO. In accordance with the gradual improvements in the analyses, the forecast skills
850 increase with the cycling frequency in most of the variables except O₃ (Figs. 10-11). Especially for the
851 forecasts of aerosols, evident gradual improvements can be seen from 0 to 24 h. From the 6-h cycling
852 experiment to the 3-h and the 1-h cycling experiment, the averaged decrease percentage of RMSE for
853 PM_{2.5} (PM₁₀) enlarges from 38.76% to 41.27% and 44.21% (27.31% to 30.17% and 32.97%); the
854 averaged increase percentage of correlation for PM_{2.5} (PM₁₀) enlarges from 42.82% to 49.51% and
855 55.58% (57.71% to 66.39% and 74.89%). To further investigate the integrated DA effect of aerosols
856 and gas phase pollutants under different cycling frequency, the TS for AQI is shown in Fig. 12. The
857 forecast of air quality is improved step by step with the increase of cycling frequency. On AQI levels
858 2-6, the TS for the ALL_1h experiment situates above the ALL_3h experiment at most of the time,

删除的内容: -
删除的内容: 8
删除的内容: 2
带格式的: 缩进: 首行缩进: 0.74 cm
带格式的: 字体: Times, 小四, 非粗体

删除的内容: 9
删除的内容: 0

删除的内容: 1

865 and followed by the ALL_6h experiment. These results indicate that the frequent IC updating is helpful
866 to further improve the forecast for most of the pollutants.

867 However, the analysis and 24-hr forecast of O₃ become worse under higher cycling frequencies
868 for this winter season (Fig. 9e and 11c). Given the analysis is at 00 UTC, the worsen analysis in the
869 experiments with higher DA frequencies (1-h, 3-h) could be mainly due to the unfavorable changes in
870 the 1-h/3-h forecasts period (starting from 23 UTC, 21 UTC), which is different from the situation in
871 the 6-h cycling experiment. As for the forecasts, the 24-hr performances starting from 00 UTC show
872 complex changes along with the forecast range: compared to the 6-h cycling experiment, the biases in
873 the experiments with higher DA frequencies decrease at 09-14 UTC but increase for other hours; the
874 RMSE and correlations in the experiments with higher DA frequencies become worse in most of the
875 hours (Fig. 11c). It should be mentioned that O₃ is a relatively short-lived chemical reactive species,
876 and takes part in highly complex and photochemical reactions in association with NO_x and VOC (Peng
877 et al. 2018, Lu et al., 2019). From this perspective, the performances of O₃ could also rely on the
878 photochemistry and the NO_x titration, in addition to the IC. Although the winter month (January 2017)
879 is investigated here when ozone photochemistry is relatively weaker compared to other seasons, the
880 photochemistry and the NO_x titration still play their roles. Accordingly, when the assimilation of NO₂
881 changes the NO₂ concentration and leave the NO and VOC unadjusted due to the absence of NO and
882 VOC measurements, two results might occur: firstly, the NO₂/VOC ratio which determine the
883 photochemical reactions and even the regime might be changed (O₃ production/loss direction might
884 change); secondly, the NO_x titration process might be changed due to the NO₂ concentration updates
885 (but no change on NO). Considering the relevant NO_x-VOC-O₃ reactions take place quickly, changing
886 the O₃ concentration in a short period, the advantage of IC DA could compete with the disadvantages

带格式的: 字体:Times, 小四, 非 粗体, 字体颜色: 自动

带格式的: 字体:Times, 小四, 非 粗体, 字体颜色: 自动

带格式的: 字体:Times, 小四, 非 粗体, 字体颜色: 自动

带格式的: 字体:Times, 小四, 非 粗体, 字体颜色: 自动

带格式的: 字体:Times, 小四, 非 粗体, 字体颜色: 自动

带格式的: 字体:Times, 小四, 非 粗体, 字体颜色: 自动

带格式的: 字体:Times, 小四, 非 粗体, 字体颜色: 自动

带格式的: 字体:Times, 小四, 非 粗体, 字体颜色: 自动

带格式的: 字体:Times, 小四, 非 粗体, 字体颜色: 自动

带格式的: 字体:Times, 小四, 非 粗体, 字体颜色: 自动

带格式的: 字体:Times, 小四, 非 粗体, 字体颜色: 自动

带格式的: 字体:Times, 小四, 非 粗体, 字体颜色: 自动

带格式的: 字体:Times, 小四, 非 粗体, 字体颜色: 自动

带格式的: 字体:Times, 小四, 非 粗体, 字体颜色: 自动

887 of the disordered photochemistry (inaccurate NO₂/VOC ratios) or the changed titration (adjusted NO₂
888 concentrations but not NO) resulting from the DA. Under this circumstance, the more frequent the O₃
889 and NO₂ were assimilated, the more incompatibilities could be brought into the related
890 photochemical/titration reactions, resulting the model performs worse in the O₃ forecasts under higher
891 cycling frequencies. It is noted that these statistics were only for the analysis at 00UTC and the 24-hr
892 forecast starting from 00UTC for winter season. Since O₃ has strong diurnal and seasonal variations,
893 more experiments and statistics at different time of the day and different season of the year should be
894 conducted in the future.

895 According to the results above, it is better to assimilate PM_{2.5}, PM₁₀, SO₂ and CO every 1 h and
896 assimilate O₃ and NO₂ every 6 h in the future applications, given the fact that the 6-h cycling
897 experiment performs the best in the O₃ forecasting (Fig. 11c) and displays no significant differences
898 in the NO₂ forecasting with experiments under higher cycling frequencies (Fig. 11b). It could also be
899 helpful to assimilate the VOC along with O₃ and NO₂ after there are corresponding observations.

900 4. Indications on further model development

901 A higher forecast skill relies on not only better working of DA, but also better performance of the
902 forecast model. To further improve the forecast skill, a crucial task is to understand the deficiencies in
903 the model, while the challenge in chemistry model diagnostic is that uncertainties are from various
904 aspects and are mixed-up in the model simulations, and the situation becomes even more complex
905 when the reaction path is not yet revealed by laboratory. However, with the help of DA, as one aspect
906 (IC) in the model is corrected by using observation as constraints, the deficiencies from other aspects
907 (e.g. chemical reactions) could be more evident, and thus there could be a better chance to diagnose

带格式的: 字体:Times, 小四, 非粗体, 字体颜色: 自动

带格式的: 字体:Times, 小四, 非粗体, 字体颜色: 自动

带格式的: 字体:Times, 小四, 非粗体, 字体颜色: 自动

带格式的: 字体:Times, 小四, 非粗体, 字体颜色: 自动

带格式的: 字体:Times, 小四, 非粗体, 字体颜色: 自动

带格式的: 字体:Times, 小四, 非粗体, 字体颜色: 自动

删除的内容: However, the analysis and forecast of O₃

becomes worse under higher cycling frequencies (Fig. 8e and

10c). As a short-lived chemical reactive species, O₃ takes

part in highly complex and rapid photochemical reactions in

association with NO₂ and VOC (Peng et al. 2018, Lu et al.,

2019). From this perspective, the performances of O₃ could

mostly rely on the rapid photochemistry, in addition to the IC.

In the DA experiments, the assimilation of NO₂ changes the

NO₂ concentration and leave the VOC unadjusted due to the

absence of VOC measurements. In result, the NO₂/VOC ratio

which determine the photochemical reactions and even

regime might be changed (O₃ production/loss direction might

change). Since the relevant NO_x-VOC-O₃ reactions take

place so quickly, changing the O₃ concentration in minutes,

the advantage of IC DA is competing with the disadvantage

of the disordered photochemistry (inaccurate NO₂/VOC

ratios) from the unadjusted VOC and the updated O₃ and

NO₂, and thus the improvement of IC DA could be consumed

quickly. Under this circumstance, the more frequent the O₃

and NO₂ were assimilated, the more incompatibilities could

be brought into the related photochemical reactions, resulting

the model performs worse in the forecast of O₃ under higher

cycling frequencies.

删除的内容:

删除的内容: 0

删除的内容: 0

934 the deficiencies in the model. Specifically, Sulfate-nitrate-ammonium (SNA) are the predominant
935 inorganic aerosol species that contribute up to 50% of total PM_{2.5} in heavily polluted events in northern
936 China (Wang et al. 2014). In addition to the normal pathways in the MOSAIC scheme, we added SO₂-
937 NO₂-NO₃ related heterogeneous reactions for high relative humidity case in WRF-Chem (Chen et al.
938 2016), which greatly improved the underestimated SNA simulations. Since the newly added reactions
939 are calculated on both the concentration of precursors (SO₂, NO₂-NO₃) and the uptake coefficients in
940 the model, after DA corrected the concentrations of the precursors (one aspect), the impacts of the
941 uptake coefficients could be more evident (the other aspect than the one corrected). Ideally, if the
942 newly added reactions depict the heterogeneous reaction processes properly, a forecast improvement
943 on the aerosols could be expected by assimilating their gaseous precursors. Based on this notion, this
944 section verifies the forecast of two specific aerosol species, sulfate (SO₄²⁻) and nitrate (NO₃⁻), against
945 a size-resolved particle observation over Beijing IUM station (in view of the assimilated SO₂ and NO₂
946 are the corresponding gaseous precursors of these aerosol species), aiming to explore the deficiencies
947 in the uptake coefficients in the newly added heterogeneous reactions, and to provide beneficial
948 indications for future model development.

949 Figure 13 presents the time series of sulfate and nitrate over Beijing IUM station. In the ALL
950 experiment, after assimilating both the PM concentrations and the gaseous precursors (SO₂, NO₂), the
951 forecasts of sulfate and nitrate become even worse than the PM₂ experiment which only assimilates
952 the PM concentrations. In the ALL experiment, sulfate experiences a decrease, accompanied by the
953 average RMSE grows from 4.32 to 4.88 μg/m³; nitrate exhibits an increase, accompanied by the
954 average RMSE grows from 8.74 to 10.12 μg/m³. However, compared to the PM₂ experiment, the
955 precursors (SO₂ and NO₂) are indeed improved. Figure 14 displays the analysis statistics of SO₂ and

删除的内容: 2

删除的内容: 3

958 NO₂ in the ALL experiment around Beijing area (red dots in Fig. 1) on January 16, the period with the
959 largest changes of sulfate and nitrate (Fig. 13). To correct the overestimated SO₂ (underestimated NO₂)
960 in the background, the DA in reduces (enhances) the model value in the ALL experiment, making it
961 closer to the observations.

962 It should be mentioned that the heterogeneous reactions are added by using the sulfate-nitrate-
963 ammonium observations as constraints to tune the “observation-best-matched” uptake coefficients
964 under the scenario without DA, in which the precursor concentrations are from pure model thus not
965 very accurate. To best match the observation, when gaseous precursors are overestimated
966 (underestimated) in the model, the uptake coefficient is tuned to low-biased (high-biased) value. In
967 result, such a coefficient may no longer be suited for the cases with DA. For instance, after DA
968 reducing the overestimated SO₂, the uptake coefficient is still relatively low and thus the reaction from
969 SO₂ to sulfate will stay at a low rate (with both low value of SO₂ and low reaction coefficient). A
970 similar result also exists for the reaction from NO₂ to nitrate. From this perspective, the negative effects
971 on sulfate and nitrate in the ALL experiment may not be hard to understand (Fig. 13). Therefore, in
972 the future chemistry development, it is necessary to develop more appropriate coefficients for different
973 gaseous precursor scenarios, in which more constraints, such as precursor and species concentrations,
974 should be provided with the help of DA technique. Accordingly, further improvements on aerosol
975 forecast could be expected by assimilating their gaseous precursors.

976 According to the results above, the DA technique provides an opportunity to identify and diagnose
977 the deficiencies in the model. By correcting the precursor concentrations through DA (one aspect), the
978 deficiency of the uptake coefficients for the SNA heterogeneous reactions (the other aspect than the
979 one corrected) is revealed. In the future, besides being used to improve the forecast skill through

删除的内容- 2

删除的内容- 2

982 updating the IC, DA could be used as another approach to reveal the necessary developments in the
983 model.

984 5. Conclusions and discussions

985 To improve the operational air quality forecasting over China, a flexible aerosol and gas phase
986 pollutants assimilation capability that can switch between different aerosol schemes is developed based
987 on the WRFDA system with 3DVAR algorithm. This flexibility is designed to address the complexity
988 of current aerosol schemes and to facilitate future chemistry developments. In this first application, the
989 assimilation capability of surface observations of six major pollutants, including PM_{2.5}, PM₁₀, SO₂,
990 NO₂, O₃, and CO, is built with MOSAIC aerosol scheme.

991 Before application in the operational air quality model, capability of the WRFDA-Chem system is
992 verified in terms of analysis and forecast performances. Using the updated system, five DA
993 experiments (assimilate different combinations of pollutants in various frequencies) were conducted
994 for January 2017, along with a control experiment without DA. Results exhibit that the WRFDA-Chem
995 system evidently improves the forecast of aerosols and gas phase pollutants. On the aspect of analysis,
996 the assimilation of different atmospheric-composition observation reduces the bias and RMSE in the
997 IC remarkably (e.g. by about ~~68%, 61%, and 30-60%~~ in the RMSE for PM_{2.5}, PM₁₀, and gas phase
998 pollutants); on the aspect of ~~forecast~~ skill, better performances are acquired up to 24 hours with about
999 10-40% (30-50%) improvements in the RMSE (correlation) for different pollutants. Among different
1000 experiments, the one assimilating all the six pollutants displays the best forecast error statistics for
1001 most of the pollutants along with the highest TS for AQI. In future applications, to get a better analysis
1002 and forecast skill in general, it is recommended to assimilate the six major pollutants simultaneously.

删除的内容: 38%, 26%, and 10-30%

删除的内容: forecast

1005 As the cycling frequency is an important aspect in the DA strategy, DA experiments with various
1006 cycling frequencies are also analyzed. Results exhibit that the responses toward IC updating are
1007 different among the pollutants. For PM_{2.5}, PM₁₀, SO₂, and CO, the forecast skills increase with the DA
1008 frequency; for O₃, compared to a better performance at the 6-h cycling frequency, its analysis at 00
1009 UTC and the following 24-hr forecast become generally worse under higher cycling frequencies for
1010 this winter season, although the biases did decrease at 09-14 UTC in the 24-hr forecast. Considering
1011 the relevant NO_x-VOC-O₃ reaction system changes the NO₂/O₃ concentration in a short period, the
1012 advantage of IC DA could compete with the disadvantages of the disordered photochemistry
1013 (inaccurate NO₂/VOC ratios) or the changed titration (adjusted NO₂ concentrations but not NO)
1014 resulting from the DA. In future applications, it is better to assimilate PM_{2.5}, PM₁₀, SO₂, and CO
1015 every 1 h. For the frequency of O₃ and NO₂ assimilation, every 6 h is the best in this winter season in
1016 our study. Since O₃ has strong diurnal and seasonal variations, more experiments and statistics at
1017 different time of the day and different season of the year should be conducted in the future. Also, it
1018 might be helpful to assimilate NO/VOC simultaneously with O₃ and NO₂ after there are corresponding
1019 measurements.

1020 By investigating the effect of assimilating gaseous precursors on the forecast of related aerosols,
1021 the deficiencies in the WRF-Chem model are further revealed. The uptake coefficients for Sulfate-
1022 Nitrate-Ammonium heterogeneous reactions in the model are found out to be not appropriate in the
1023 applications with gaseous precursors (SO₂ and NO₂) assimilations, since they were originally tuned
1024 under the gaseous precursor scenarios without DA and the biases from the two aspects (SNA reactions
1025 and IC DA) were just compensated. In the future chemistry development, it is necessary to develop

带格式的: 缩进: 首行缩进: 0 cm

带格式的: 字体:Times,小四,非粗体,字体颜色:自动
带格式的: 字体:Times,小四,非粗体,字体颜色:自动
带格式的: 字体:Times,小四,非粗体,字体颜色:自动
带格式的: 字体:Times,小四,非粗体,字体颜色:自动
带格式的: 字体:Times,小四,非粗体,字体颜色:自动
带格式的: 字体:Times,小四,非粗体,字体颜色:自动
带格式的: 字体:Times,小四,非粗体,字体颜色:自动
带格式的: 字体:Times,小四,非粗体,字体颜色:自动
带格式的: 字体:Times,小四,非粗体,字体颜色:自动
带格式的: 字体:Times,小四,非粗体,字体颜色:自动
带格式的: 字体:Times,小四,非粗体,字体颜色:自动
带格式的: 字体:Times,小四,非粗体,字体颜色:自动

删除的内容: 为 O₃, although improvements are acquired at the 6-h cycling frequency, **the analysis at 00 UTC and 24-hr forecast (starting from 00 UTC) of O₃ becomes generally worse under higher cycling frequencies for this winter season, although biases did decrease at 09-14 UTC for 24-hr forecast. Considering the relevant NO_x-VOC-O₃ reaction system, changing the NO₂/O₃ concentration in a short period, the advantage of IC DA is competing with the disadvantage of the disordered photochemistry (inaccurate NO₂/VOC ratios) or changed titration (adjusted NO₂ concentrations but not NO) from the unadjusted VOC/NO and the updated O₃/NO₂ by DA, the advantage of more frequent IC DA could be consumed by the disordered photochemistry (inaccurate NO₂/VOC** [1]

带格式的: 字体:(默认) Times New Roman, 粗体
带格式的: 字体:小四
带格式的: 字体:小四,粗体
带格式的: 字体:小四,粗体
带格式的: 字体:小四,粗体
带格式的: 字体:小四
带格式的: 字体:小四,粗体
带格式的: 字体:小四,粗体
带格式的: 字体:小四,粗体
带格式的: 字体:小四,粗体
带格式的: 字体:(默认) Times New Roman, 粗体
带格式的: 字体:(默认) Times New Roman, 小四,粗体
带格式的: 字体:(默认) Times New Roman, 粗体
带格式的: 字体:小四
带格式的: 字体:(默认) Times New Roman, 粗体

1065 appropriate coefficients for different gaseous precursor scenarios, in which more constraints, such as
1066 precursor and species concentrations, should be provided with the help of DA technique.

1067 As for the significantly underestimated PMcoarse in the model, the results might relate to the
1068 missing emissions under current situations. Different from the United states or European countries that
1069 national emission inventories are provided and updated frequently by the government (e.g. US
1070 National Emission Inventory NEI 05-08-11-14-17), the publicly available emission inventories for
1071 China are mainly established by several scientific research groups. In result, the uncertainties of the
1072 publicly available emission inventories in China are relatively larger compared with others (US,
1073 European countries), and it's a known problem that the fugitive dust emissions over the whole of China
1074 is still lack, which might cause the underestimated PMcoarse simulation in the model.

带格式的: 字体:Times, 小四, 非 粗体
带格式的: 缩进: 首行缩进: 0.74 cm

1075 Contributed by the flexible aerosol assimilation capability of the WRFDA-Chem system,
1076 development for other aerosol schemes targeting different regions in Asia is undergoing. In the next
1077 step, a study will focus on assimilating chemical observations from different observing platforms, such
1078 as satellite AOD observations, which contain more information over the areas with sparse surface
1079 observations. In addition, more advanced DA techniques, such as 4DVAR and Hybrid DA, could be
1080 taken into consideration in further developing the aerosol/chemical DA system.

删除的内容: s

1081 Code and data availability

1082 The data used in the figures and the developed WRFDA-Chem codes are available from WS upon
1083 request.

带格式的: 缩进: 首行缩进: 0.74 cm

带格式的: 字体:(默认) Times New Roman

1085 **Author contributions**

1086 WS and ZL conducted development of DA system. ZL, DC, WS, and MC designed research, WS
1087 performed experiments and analyzed results, PZ provided PM species observations, and WS and DC
1088 wrote the paper with contributions from all co-authors.

1089 **Acknowledgement**

1090 This work was supported by the National Key R&D Program on Monitoring, Early Warning and
1091 Prevention of Major Natural Disasters under grant (2017YFC1501406), and Basic R&D special fund
1092 for central level, scientific research institutes (IUMKYSZHZJ201701, IUMKY201807) of China.
1093 NCAR is sponsored by the US National Science Foundation.

1094 **Competing interests**

1095 The authors declare that they have no conflict of interest.

带格式的: 缩进: 首行缩进: 0 字符
带格式的

1096 **References**

1097 Bannister, R., 2017: A review of operational methods of variational and ensemble-variational data
1098 assimilation. *Quarterly Journal of the Royal Meteorological Society*, **143**, 607-633.
1099 Chen, D., Z. Liu, J. Fast, and J. Ban, 2016: Simulations of sulfate–nitrate–ammonium (SNA) aerosols
1100 during the extreme haze events over northern China in October 2014. *Atmospheric Chemistry and*
1101 *Physics*, **16**, 10707-10724.

1102 Chen, D., Z. Liu, J. Ban, P. Zhao, and M. Chen, 2019: Retrospective analysis of 2015–2017 wintertime
1103 PM 2.5 in China: response to emission regulations and the role of meteorology. *Atmospheric*
1104 *Chemistry and Physics*, **19**, 7409-7427.

1105 Chen, F., and J. Dudhia, 2001: Coupling an advanced land surface–hydrology model with the Penn
1106 State–NCAR MM5 modeling system. Part I: Model implementation and sensitivity. *Monthly*
1107 *Weather Review*, **129**, 569-585.

1108 Chou, M.-D., and M. J. Suarez, 1994: An efficient thermal infrared radiation parameterization for use
1109 in general circulation models.

1110 Descombes, G., T. Auligné, F. Vandenberghe, D. Barker, and J. Barre, 2015: Generalized background
1111 error covariance matrix model (GEN_BE v2. 0). *Geoscientific Model Development*, **8**, 669-696.

1112 Fan, S., and Coauthors, 2016: Introduction of Rapid-refresh Multi-scale Analysis and Prediction
1113 System-short time (RMAP-ST) over Northern China (in Chinese). *33th Annual Meeting of*
1114 *Chinese Meteorological Society*.

1115 Fast, J. D., and Coauthors, 2006: Evolution of ozone, particulates, and aerosol direct radiative forcing
1116 in the vicinity of Houston using a fully coupled meteorology-chemistry-aerosol model. *Journal*
1117 *of Geophysical Research: Atmospheres*, **111**.

1118 Fu, Y., H. Liao, and Y. Yang, 2019: Interannual and decadal changes in tropospheric ozone in China
1119 and the associated chemistry-climate interactions: A review. *Advances in Atmospheric Sciences*,
1120 **36**, 975-993.

1121 Grell, G. A., and D. Dévényi, 2002: A generalized approach to parameterizing convection combining
1122 ensemble and data assimilation techniques. *Geophysical Research Letters*, **29**, 38-31-38-34.

1123 Grell, G. A., S. E. Peckham, R. Schmitz, S. A. McKeen, G. Frost, W. C. Skamarock, and B. Eder,
1124 2005: Fully coupled “online” chemistry within the WRF model. *Atmospheric Environment*, **39**,
1125 6957-6975.

1126 He, K., 2012: Multi-resolution emission Inventory for China (MEIC): model framework and 1990–
1127 2010 anthropogenic emissions, presented on the international Global Atmospheric Chemistry
1128 Conference, 17–21 September 2012, Beijing, China.

1129 Hong, S.-Y., Y. Noh, and J. Dudhia, 2006: A new vertical diffusion package with an explicit treatment
1130 of entrainment processes. *Monthly weather review*, **134**, 2318-2341.

1131 Huang, X., Y. Song, C. Zhao, M. Li, T. Zhu, Q. Zhang, and X. Zhang, 2014: Pathways of sulfate
1132 enhancement by natural and anthropogenic mineral aerosols in China. *Journal of Geophysical*
1133 *Research: Atmospheres*, **119**, 14,165-114,179.

1134 Jiang, Z., Z. Liu, T. Wang, C. S. Schwartz, H. C. Lin, and F. Jiang, 2013: Probing into the impact of
1135 3DVAR assimilation of surface PM10 observations over China using process analysis. *Journal*
1136 *of Geophysical Research: Atmospheres*, **118**, 6738-6749.

1137 Kumar, A., and P. Goyal, 2011: Forecasting of daily air quality index in Delhi. *Science of the Total*
1138 *Environment*, **409**, 5517-5523.

1139 Lei, Y., Q. Zhang, K. He, and D. Streets, 2011: Primary anthropogenic aerosol emission trends for
1140 China, 1990–2005. *Atmospheric Chemistry and Physics*, **11**, 931-954.

1141 Li, M., and Coauthors, 2014: Mapping Asian anthropogenic emissions of non-methane volatile organic
1142 compounds to multiple chemical mechanisms. *Atmos. Chem. Phys*, **14**, 5617-5638.

1143 Liu, Z., Q. Liu, H. C. Lin, C. S. Schwartz, Y. H. Lee, and T. Wang, 2011: Three-dimensional
1144 variational assimilation of MODIS aerosol optical depth: Implementation and application to a
1145 dust storm over East Asia. *Journal of Geophysical Research: Atmospheres*, **116** (D23).

1146 Lu, X., and Coauthors, 2019: Exploring 2016–2017 surface ozone pollution over China: source
1147 contributions and meteorological influences. *Atmospheric Chemistry and Physics*, **19**, 8339–8361.

1148 McHenry, J. N., J. M. Vukovich, and N. C. Hsu, 2015: Development and implementation of a remote-
1149 sensing and in situ data-assimilating version of CMAQ for operational PM_{2.5} forecasting. Part
1150 1: MODIS aerosol optical depth (AOD) data-assimilation design and testing. *Journal of the Air
1151 & Waste Management Association*, **65**, 1395–1412.

1152 McKeen, S., and Coauthors, 2009: An evaluation of real-time air quality forecasts and their urban
1153 emissions over eastern Texas during the summer of 2006 Second Texas Air Quality Study field
1154 study. *Journal of Geophysical Research: Atmospheres*, **114**.

1155 Mlawer, E. J., S. J. Taubman, P. D. Brown, M. J. Iacono, and S. A. Clough, 1997: Radiative transfer
1156 for inhomogeneous atmospheres: RRTM, a validated correlated-k model for the longwave.
1157 *Journal of Geophysical Research: Atmospheres*, **102**, 16663–16682.

1158 Nie, W., and Coauthors, 2014: Polluted dust promotes new particle formation and growth. *Scientific
1159 reports*, **4**, 6634.

1160 Pang, J., Z. Liu, X. Wang, J. Bresch, J. Ban, D. Chen, and J. Kim, 2018: Assimilating AOD retrievals
1161 from GOCI and VIIRS to forecast surface PM_{2.5} episodes over Eastern China. *Atmospheric
1162 environment*, **179**, 288–304.

1163 Peng, Z., Z. Liu, D. Chen, and J. Ban, 2017: Improving PM 2.5 forecast over China by the joint
1164 adjustment of initial conditions and source emissions with an ensemble Kalman filter.
1165 *Atmospheric Chemistry and Physics*, **17**, 4837-4855.

1166 Peng, Z., and Coauthors, 2018: The impact of multi-species surface chemical observation assimilation
1167 on air quality forecasts in China. *Atmospheric Chemistry and Physics*, **18**, 17387-17404.

1168 Sandu, A., and T. Chai, 2011: Chemical data assimilation—An overview. *Atmosphere*, **2**, 426-463.

1169 Schutgens, N., T. Miyoshi, T. Takemura, and T. Nakajima, 2010: Applying an ensemble Kalman filter
1170 to the assimilation of AERONET observations in a global aerosol transport model. *Atmospheric*
1171 *Chemistry and Physics*, **10**, 2561-2576.

1172 Schwartz, C. S., Z. Liu, H. C. Lin, and S. A. McKeen, 2012: Simultaneous three-dimensional
1173 variational assimilation of surface fine particulate matter and MODIS aerosol optical depth.
1174 *Journal of Geophysical Research: Atmospheres*, **117**.

1175 Sekiyama, T., T. Tanaka, A. Shimizu, and T. Miyoshi, 2010: Data assimilation of CALIPSO aerosol
1176 observations. *Atmospheric Chemistry and Physics*, **10**, 39-49.

1177 Su, J., P. Zhao, and Q. Dong, 2018: Chemical compositions and liquid water content of size-resolved
1178 aerosol in Beijing. *Aerosol Air Qual. Res*, **18**, 680-692.

1179 Tang, X., J. Zhu, Z. Wang, and A. Gbaguidi, 2011: Improvement of ozone forecast over Beijing based
1180 on ensemble Kalman filter with simultaneous adjustment of initial conditions and emissions.
1181 *Atmospheric Chemistry and Physics*, **11**, 12901-12916.

1182 Tang, X., and Coauthors, 2013: Inversion of CO emissions over Beijing and its surrounding areas with
1183 ensemble Kalman filter. *Atmospheric environment*, **81**, 676-686.

1184 Tao, J., L. Zhang, J. Gao, H. Wang, F. Chai, and S. Wang, 2015: Aerosol chemical composition and
1185 light scattering during a winter season in Beijing. *Atmospheric Environment*, **110**, 36-44.

1186 Wang, G., and Coauthors, 2016: Persistent sulfate formation from London Fog to Chinese haze.
1187 *Proceedings of the National Academy of Sciences*, **113**, 13630-13635.

1188 Wang, L., and Coauthors, 2013: The 2013 severe haze over the southern Hebei, China: model
1189 evaluation, source apportionment, and policy implications. *Atmospheric Chemistry & Physics*
1190 *Discussions*, **13**.

1191 Wang, Y., and Coauthors, 2014: Enhanced sulfate formation during China's severe winter haze episode
1192 in January 2013 missing from current models. *Journal of Geophysical Research: Atmospheres*,
1193 **119**, 10,425-410,440.

1194 Wild, O., X. Zhu, and M. J. Prather, 2000: Fast-J: Accurate simulation of in-and below-cloud
1195 photolysis in tropospheric chemical models. *Journal of Atmospheric Chemistry*, **37**, 245-282.

1196 Xie, Y., and Coauthors, 2015: Enhanced sulfate formation by nitrogen dioxide: Implications from in
1197 situ observations at the SORPES station. *Journal of Geophysical Research: Atmospheres*, **120**,
1198 12679-12694.

1199 Yu, M., S. Miao, and H. Zhang, 2018: Uncertainties in the Impact of Urbanization on Heavy Rainfall:
1200 Case Study of a Rainfall Event in Beijing on 7 August 2015. *Journal of Geophysical Research:*
1201 *Atmospheres*, **123**, 6005-6021.

1202 Zaveri, R. A., and L. K. Peters, 1999: A new lumped structure photochemical mechanism for large-
1203 scale applications. *Journal of Geophysical Research: Atmospheres*, **104**, 30387-30415.

1204 Zaveri, R. A., R. C. Easter, J. D. Fast, and L. K. Peters, 2008: Model for simulating aerosol interactions
1205 and chemistry (MOSAIC). *Journal of Geophysical Research: Atmospheres*, **113**.

1206 Zhang, Q., and Coauthors, 2009: Asian emissions in 2006 for the NASA INTEX-B mission.
1207 *Atmospheric Chemistry and Physics*, **9**, 5131-5153.
1208 Zheng, B., and Coauthors, 2015: Heterogeneous chemistry: a mechanism missing in current models to
1209 explain secondary inorganic aerosol formation during the January 2013 haze episode in North
1210 China. *Atmospheric Chemistry and Physics (Online)*, **15**.
1211 Zheng, S., C.-X. Cao, and R. P. Singh, 2014: Comparison of ground based indices (API and AQI) with
1212 satellite based aerosol products. *Science of the Total Environment*, **488**, 398-412.

1213 **Tables and Figures**

1214 **Table 1.** WRF-Chem model configurations.

1215 **Table 2.** The detail setting of six experiments and the purposes.

1216 **Table 3.** Averaged bias (units: $\mu\text{g}/\text{m}^3$), RMSE (units: $\mu\text{g}/\text{m}^3$), and correlation over forecast hour 0-24
1217 h for different variables and different experiments. The statistics for gas phase pollutants in PM1 and
1218 PM2 experiments are highly close to the results in NODA experiment, and thus leave with blank in
1219 the table.

1220 **Figure 1.** Computation domain. Dots depict surface observations with 531 stations spreading over
1221 China. The red dots indicate the observations around Beijing. The green dot indicates the IUM station.
1222 **Figure 2.** Background error standard deviations of aerosol species in the (a) 1st size bin, (b) 2nd size
1223 bin, (c) 3rd size bin, (d) 4th size bin, and of (e) gas pollutants. The units for the x-axis are $\mu\text{g m}^{-3}$ for
1224 (a)-(d) and ppm for (e). The left y-axis denotes the model level, and the right y-axis denotes the vertical
1225 height (units: km).

删除的内容: **Figure 1.** Computation domain. Dots depict surface observations with 531 stations spreading over China. The red dots indicate the observations around Beijing. . .

Figure 2

带格式的: 字体:Times, 小四

带格式的: 字体:Times, 小四, 非 粗体

带格式的: 字体:Times, 小四, 非 粗体

1230 **Figure 3.** Averaged bias (color bar, left y-axis) and RMSE (hallow bar, right y-axis) of the analysis at
1231 00 UTC over January 1-31, 2017 for (a) PM_{2.5}, (b) PM₁₀, (c) SO₂, (d) NO₂, (e) O₃ and (f) CO in different
1232 experiments, verified against the surface observations of 531 stations in China. The blue, red, green
1233 and gray shaded bars denote the bias of the experiment NODA, PM1, PM2, ALL, respectively; the
1234 corresponding hallow bars denote the RMSE of these experiments. Units of the y-axis are $\mu\text{g}/\text{m}^3$ in
1235 Figs. 3a-e and mg/m^3 in Fig. 3f.

删除的内容: 2

1236 **Figure 4.** Averaged PMcoarse (PM_{10-2.5}, units: $\mu\text{g}/\text{m}^3$) at 00 UTC over January 1-31, 2017 in (a)
1237 observation and four experiments (b) NODA, (c) PM1, (d) PM2, (e) ALL, and (f) averaged bias (units:
1238 $\mu\text{g}/\text{m}^3$) for PMcoarse in different experiments as a function of forecast range (the blue, red, green and
1239 gray lines denote the results of experiment NODA, PM1, PM2, ALL, respectively), verified against
1240 the surface observations of 531 stations in China. The numbers on the top of each panel denote the
1241 average PMcoarse concentrations over 531 stations (units: $\mu\text{g}/\text{m}^3$).

删除的内容: 2

删除的内容: 2

删除的内容: 3

1242 **Figure 5.** Vertical profile of the analysis at 00 UTC over January 1-31, 2017 for (a) PM_{2.5}, (b) PM₁₀,
1243 (c) SO₂, (d) NO₂, (e) O₃, and (f) CO in different experiments, averaged over the 531 surface stations
1244 in China. The blue, red, green and gray lines denote the results of experiment NODA, PM1, PM2, and
1245 ALL, respectively. Units of the y-axis are $\mu\text{g}/\text{m}^3$ in Figs. 5a-e and mg/m^3 in Fig. 5f.

删除的内容: 4

1246 **Figure 6.** Averaged bias (units: $\mu\text{g}/\text{m}^3$), RMSE (units: $\mu\text{g}/\text{m}^3$), and correlation for (a) PM_{2.5} and (b)
1247 PM₁₀ in different experiments as a function of forecast range, verified against the surface observations
1248 of 531 stations in China. The blue, red, green and gray lines denote the results of experiment NODA,
1249 PM1, PM2, ALL, respectively.

删除的内容: 4

删除的内容: 4

删除的内容: 5

1250 **Figure 7.** Same as Fig. 6, but for the forecast of (a) SO₂, (b) NO₂, (c) O₃ (units: $\mu\text{g}/\text{m}^3$), and (d) CO
1251 (units: mg/m^3).

删除的内容: 6

删除的内容: 5

1262 **Figure 8**, Averaged threat score (TS) for Air Quality Index (AQI) from AQI level 1 to level 6 (a-f) in
 1263 different experiments as a function of forecast range, verified against the surface observations of 531
 1264 stations in China. The blue, red, green and gray lines denote the results of experiment NODA, PM1,
 1265 PM2, and ALL, respectively. The numbers on the right of each panel denote the averaged TS from 0
 1266 to 24 h for different experiments.

1267 **Figure 9**, Same as Fig. 3, but for the experiments of NODA, ALL_6h, ALL_3h, ALL_1h, respectively.
 1268 Units of the y-axis are $\mu\text{g}/\text{m}^3$ in Figs. 9a-e and mg/m^3 in Fig. 9f.

1269 **Figure 10**, Averaged bias (units: $\mu\text{g}/\text{m}^3$), RMSE (units: $\mu\text{g}/\text{m}^3$), and correlation for (a) $\text{PM}_{2.5}$ and (b)
 1270 PM_{10} in different experiments as a function of forecast range, verified against the surface observations
 1271 of 531 stations in China. The blue, red, green and gray lines denote the results of experiment NODA,
 1272 ALL_6h, ALL_3h, and ALL_1h, respectively.

1273 **Figure 11**, Same as Fig. 10, but for the forecast of (a) SO_2 , (b) NO_2 , (c) O_3 (units: $\mu\text{g}/\text{m}^3$), and (d) CO
 1274 (units: mg/m^3).

1275 **Figure 12**, Same as Fig. 8, but for the experiments of NODA, ALL_6h, ALL_3h, ALL_1h, respectively.

1276 **Figure 13**, Time series of (a) sulfate, (b) nitrate over January 14-20, verified against the size-resolved
 1277 particle observation at IUM station (units: $\mu\text{g}/\text{m}^3$). The gray, blue and red lines denote the observation
 1278 and the results of experiment PM2 and ALL, respectively. The numbers on the right of each panel
 1279 denote the averaged RMSE over January 14-20 for different experiments.

1280 **Figure 14**, Averaged scatter plot of (a, c) observation versus background and (b, d) observation versus
 1281 analysis for (a, b) SO_2 and (c, d) NO_2 around Beijing area (red dots in Fig. 1) on January 16. The
 1282 numbers on the title denote the accumulated numbers of the used observations around Beijing area
 1283 during January 16 (1600 UTC, 1606 UTC, 1612 UTC, and 1618 UTC).

删除的内容: 7

删除的内容: 8

删除的内容: 2

删除的内容: 8

删除的内容: 8

删除的内容: 9

删除的内容: 0

删除的内容: 9

删除的内容: 1

带格式的: 字体:非 粗体

删除的内容: 7

带格式的: 两端对齐, 行距: 1.5 倍行距

删除的内容: 2

带格式的: 字体:非 粗体

带格式的

带格式的

带格式的: 字体:Times

删除的内容: 3

带格式的: 字体:非 粗体

带格式的: 字体:小四

带格式的: 字体:小四

删除的内容: .

Tab

Table 1. WRF-Chem model configurations.

Aerosol scheme	MOSAIC (four bins, Zaveri et al. (2008))
Photolysis scheme	Fast-J (Wild et al. 2000)
Gas-phase chemistry	CBM-Z (Zaveri and Peters 1999)
Cumulus parameterization	Grell 3-D scheme Goddard Space Flight Center short-wave radiation scheme
Short-wave radiation	(Chou and Suarez 1994)
Long-wave radiation	RRTM (Mlawer et al. 1997)
Microphysics	Single-moment 6-class scheme (Grell and Dévényi 2002)
Land-surface model (LSM)	NOAH LSM (Chen and Dudhia 2001)
Boundary-layer scheme	YSU (Hong et al. 2006)
Meteorology initial and boundary conditions	GFS analysis and forecast every 6 h
Initial condition for chemical species	11-day spin-up
Boundary conditions for chemical species	Averages of mid-latitude aircraft profiles
Dust and sea salt emissions	GOCART

1300

Table 2. The detail setting of six experiments and the purposes

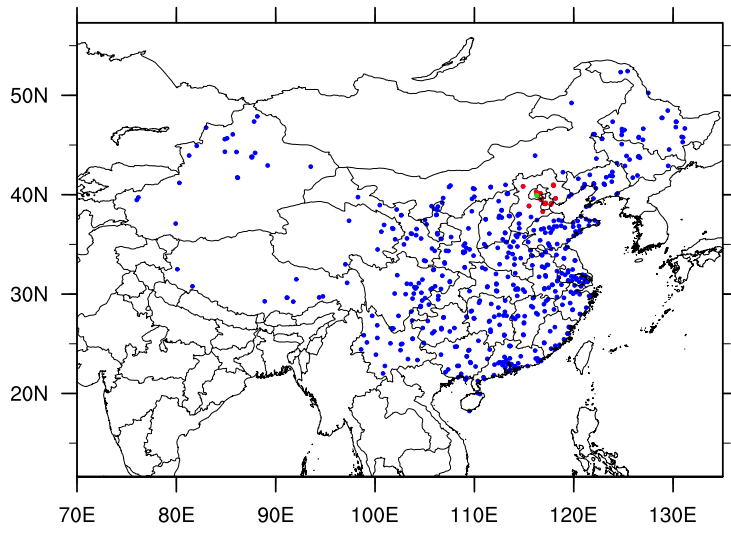
Experiments	PM _{2.5} assimilation	PM _{10-2.5} assimilation	Gas phase (SO ₂ , NO ₂ , O ₃ , CO) assimilation	Assimilated time (UTC)	Purposes for forecast performances
NODA	No	No	No	--	Control simulation
PM1	Yes	No	No	00, 06, 12, 18	Basic PM _{2.5} assimilation
PM2	Yes	Yes	No	00, 06, 12, 18	PM _{2.5} and PM _{10-2.5} assimilation
ALL	Yes	Yes	Yes	00, 06, 12, 18	Aerosol and precursor simultaneously assimilation
ALL_3h	Yes	Yes	Yes	00, 03, 06, 09, 12, 15, 18, 21	Different assimilation frequencies on forecast performances
ALL_1h	Yes	Yes	Yes	0-23, every hour	

1301

1302 **Table 3.** Averaged bias (units: $\mu\text{g}/\text{m}^3$), RMSE (units: $\mu\text{g}/\text{m}^3$), and correlation over forecast hour 0-24
 1303 h for different variables and different experiments. The statistics for gas phase pollutants in PM1 and
 1304 PM2 experiments are highly close to the results in NODA experiment, and thus leave with blank in
 1305 the table.

		NODA	PM1	PM2	ALL
PM _{2.5}	Bias	31.17	8.78	8.39	9.36
	RMSE	88.99	53.93	54.35	54.49
	Correlation	0.41	0.59	0.58	0.59
PM ₁₀	Bias	-1.13	-22.73	-15.43	-14.41
	RMSE	98.5	74.41	71.9	71.6
	Correlation	0.36	0.54	0.56	0.56
SO ₂	Bias	6.67	-	-	3.78
	RMSE	44.11	-	-	38.18
	Correlation	0.29	-	-	0.4
NO ₂	Bias	-2.87	-	-	-1.66
	RMSE	25.61	-	-	24.26
	Correlation	0.48	-	-	0.52
O ₃	Bias	-3.22	-	-	-0.84
	RMSE	31.96	-	-	28.36
	Correlation	0.29	-	-	0.41
CO	Bias	-0.73	-	-	-0.19
	RMSE	1.13	-	-	0.75
	Correlation	0.28	-	-	0.57

1306

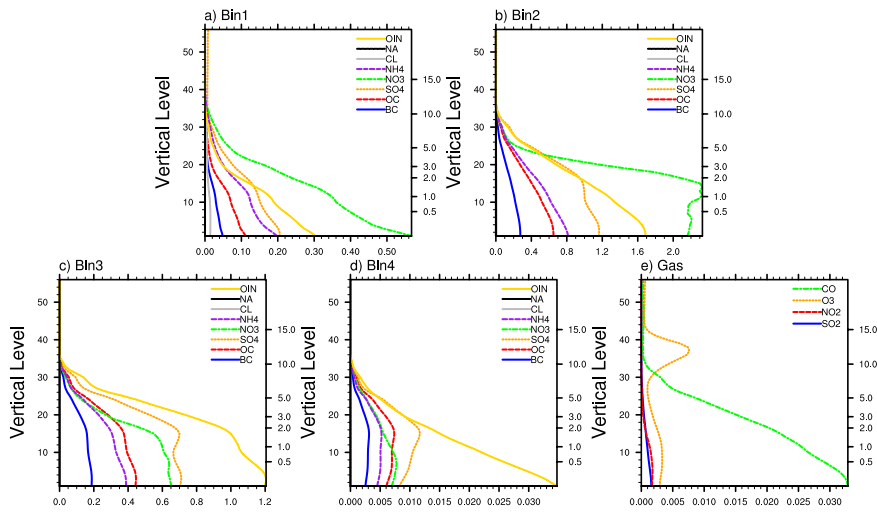


1307

1308 **Figure 1.** Computation domain. Dots depict surface observations with 531 stations spreading over

1309 China. The red dots indicate the observations around Beijing. The green dot indicates the IUM station.

1310

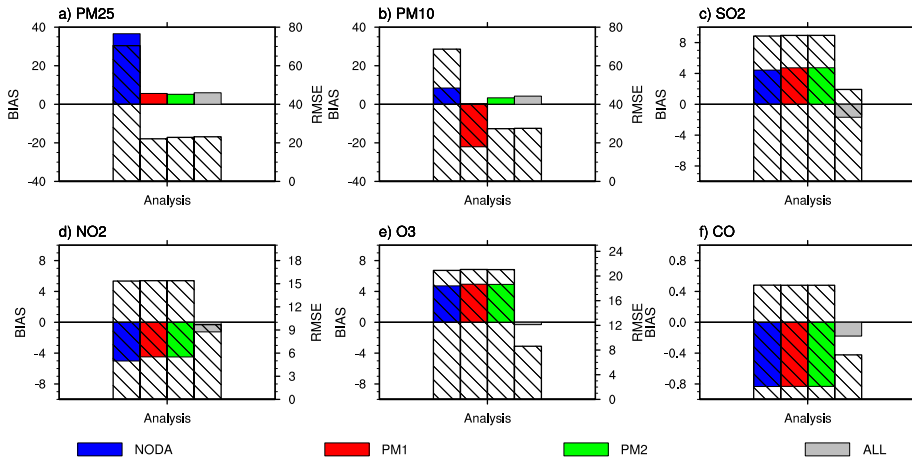


1311 **Figure 2.** Background error standard deviations of aerosol species in the (a) 1st size bin, (b) 2nd size
 1312 bin, (c) 3rd size bin, (d) 4th size bin, and of (e) gas pollutants. The units for the x-axis are $\mu\text{g m}^{-3}$ for
 1313 (a)-(d) and ppm for (e). The left y-axis denotes the model level, and the right y-axis denotes the vertical
 1314 height (units: km).
 1315
 1316

带格式的: 字体:Times, 小四

带格式的: 字体:Times, 小四, 非 粗体

带格式的: 字体:Times, 小四, 非 粗体



1317

1318 **Figure 3.** Averaged bias (color bar, left y-axis) and RMSE (hallow bar, right y-axis) of the analysis at
 1319 00 UTC over January 1-31, 2017 for (a) PM_{2.5}, (b) PM₁₀, (c) SO₂, (d) NO₂, (e) O₃ and (f) CO in different
 1320 experiments, verified against the surface observations of 531 stations in China. The blue, red, green
 1321 and gray shaded bars denote the bias of the experiment NODA, PM1, PM2, ALL, respectively; the
 1322 corresponding hallow bars denote the RMSE of these experiments. Units of the y-axis are $\mu\text{g}/\text{m}^3$ in

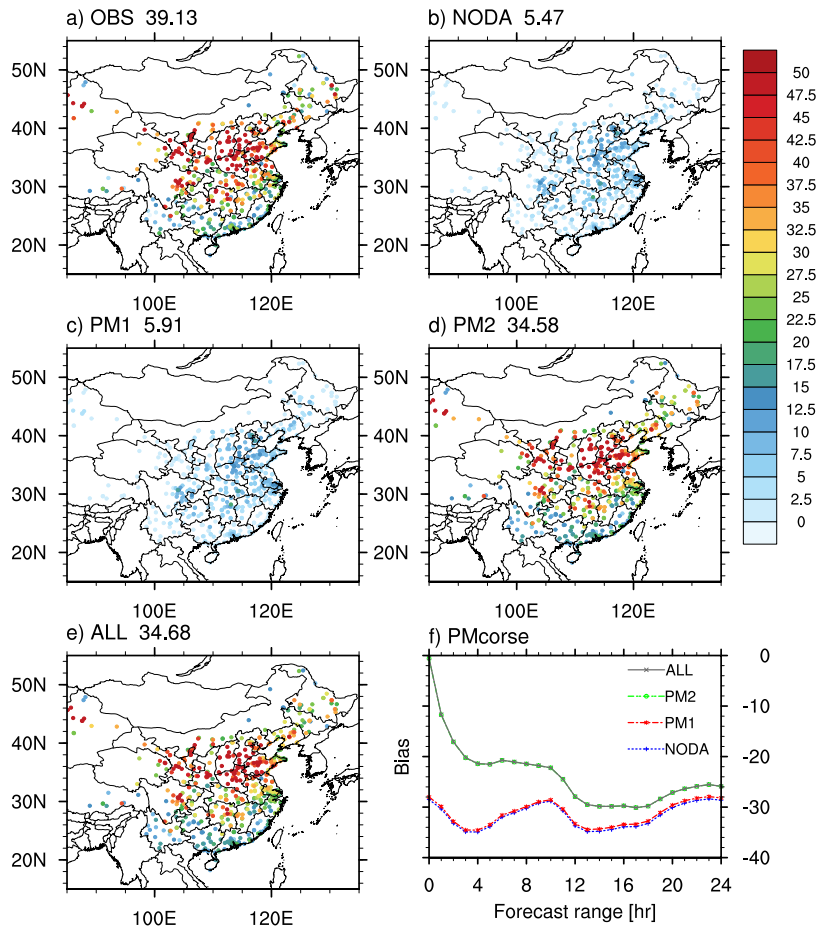
删除的内容: 2

1323 Figs. 3a-e and mg/m^3 in Fig. 3f.

1324

删除的内容: 2

删除的内容: 2



1328

1329

Figure 4. Averaged PMcoarse ($PM_{10-2.5}$, units: $\mu\text{g}/\text{m}^3$) at 00 UTC over January 1-31, 2017 in (a) observation and four experiments (b) NODA, (c) PM1, (d) PM2, (e) ALL, and (f) averaged bias (units: $\mu\text{g}/\text{m}^3$) for PMcoarse in different experiments as a function of forecast range (the blue, red, green and gray lines denote the results of experiment NODA, PM1, PM2, ALL, respectively), verified against the surface observations of 531 stations in China. The numbers on the top of each panel denote the average PMcoarse concentrations over 531 stations (units: $\mu\text{g}/\text{m}^3$).

1330

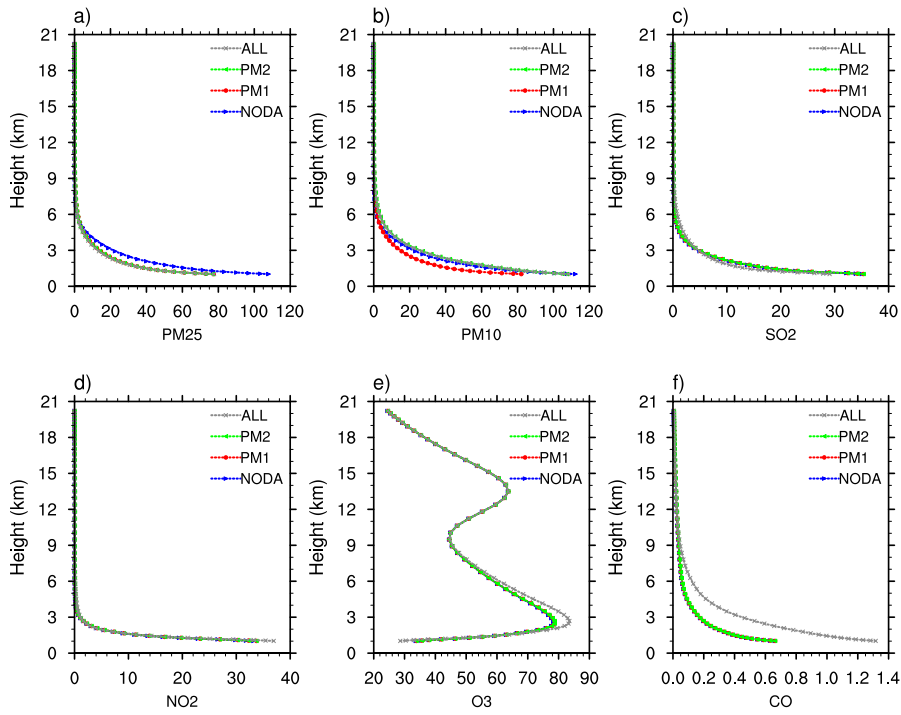
1331

1332

1333

1334

删除的内容: 3



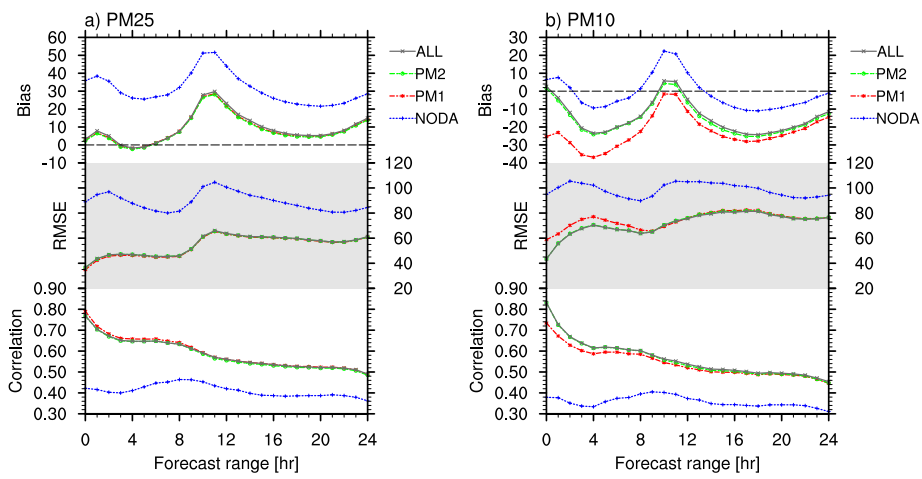
1336

1337 **Figure 5.** Vertical profile of the analysis at 00 UTC over January 1-31, 2017 for (a) PM_{2.5}, (b) PM₁₀,
 1338 (c) SO₂, (d) NO₂, (e) O₃, and (f) CO in different experiments, averaged over the 531 surface stations
 1339 in China. The blue, red, green and gray lines denote the results of experiment NODA, PM1, PM2, and
 1340 ALL, respectively. Units of the y-axis are $\mu\text{g}/\text{m}^3$ in Figs. 5a-e and mg/m^3 in Fig. 5f.

删除的内容: 4

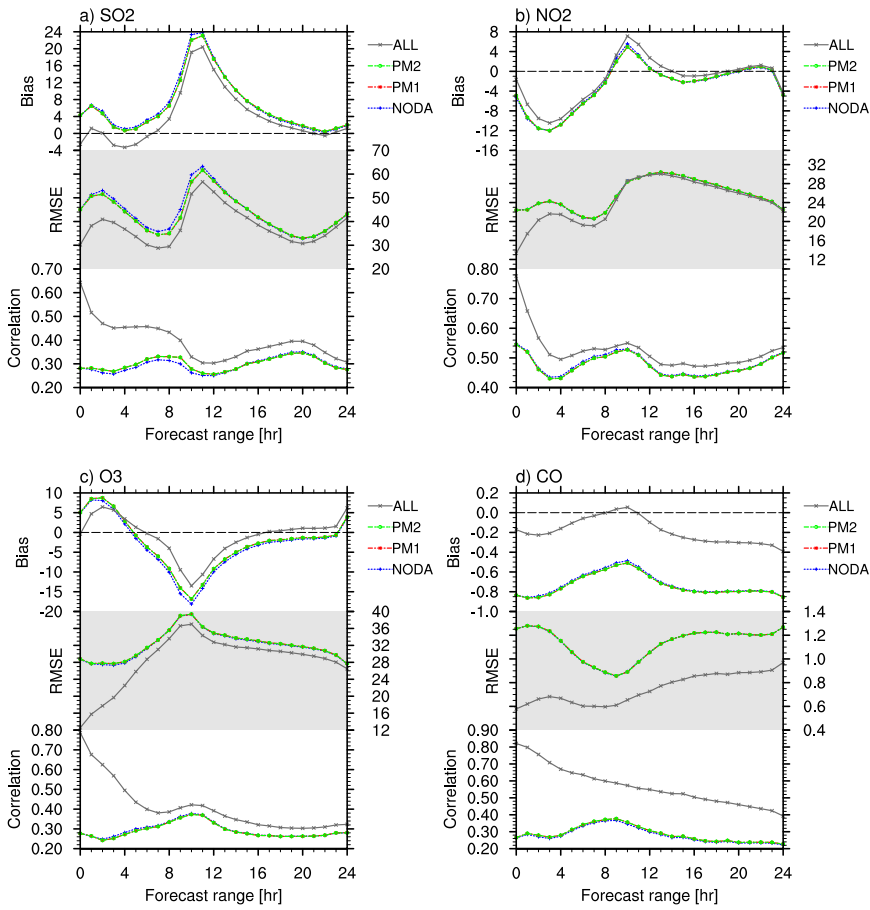
删除的内容: 4

删除的内容: 4



1344
 1345 **Figure 6.** Averaged bias (units: $\mu\text{g}/\text{m}^3$), RMSE (units: $\mu\text{g}/\text{m}^3$), and correlation for (a) $\text{PM}_{2.5}$ and (b)
 1346 PM_{10} in different experiments as a function of forecast range, verified against the surface observations
 1347 of 531 stations in China. The blue, red, green and gray lines denote the results of experiment NODA,
 1348 PM1, PM2, ALL, respectively.

删除的内容: 5

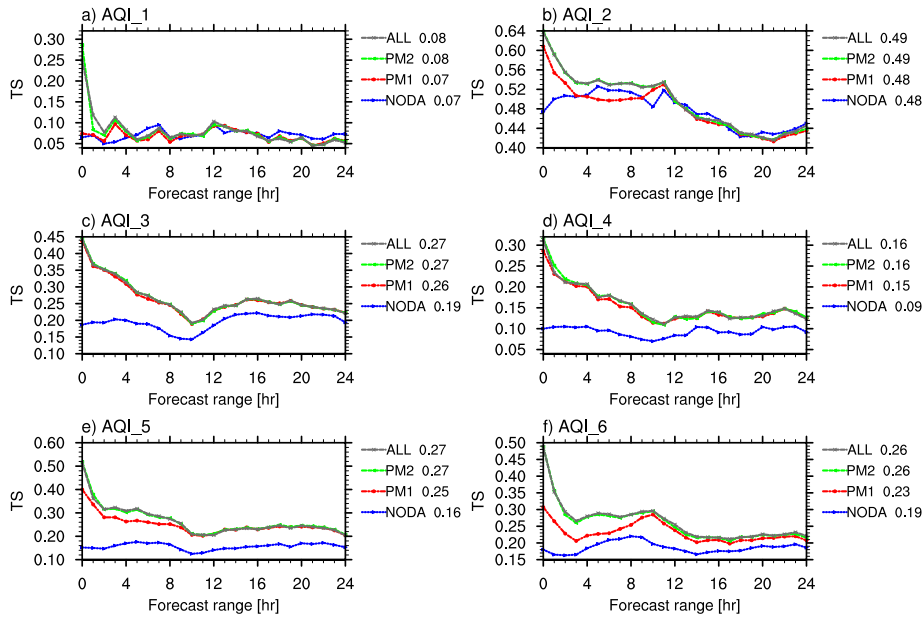


1350

1351 **Figure 7.** Same as Fig. 6, but for the forecast of (a) SO₂, (b) NO₂, (c) O₃ (units: μg/m³), and (d) CO

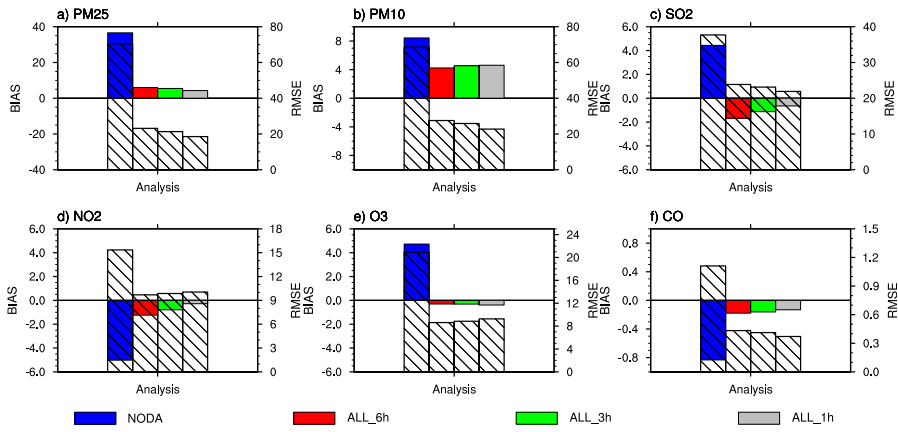
1352 (units: mg/m³).

删除的内容: 6
删除的内容: 5



1355
 1356 **Figure 8.** Averaged threat score (TS) for Air Quality Index (AQI) from AQI level 1 to level 6 (a-f) in
 1357 different experiments as a function of forecast range, verified against the surface observations of 531
 1358 stations in China. The blue, red, green and gray lines denote the results of experiment NODA, PM1,
 1359 PM2, and ALL, respectively. The numbers on the right of each panel denote the averaged TS from 0
 1360 to 24 h for different experiments.

删除的内容: 7



1362

1363

Figure 9, Same as Fig. 3, but for the experiments of NODA, ALL_6h, ALL_3h, ALL_1h, respectively.

删除的内容: 8

1364

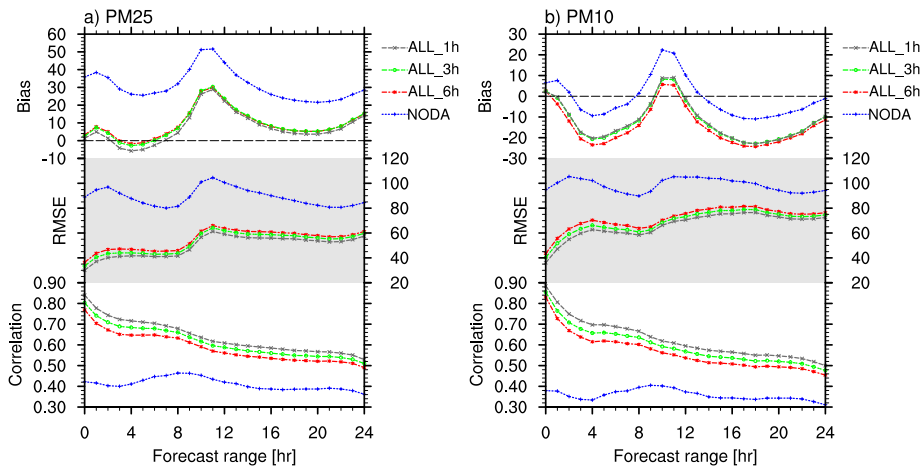
Units of the y-axis are $\mu\text{g}/\text{m}^3$ in Figs. 9a-e and mg/m^3 in Fig. 9f.

删除的内容: 2

1365

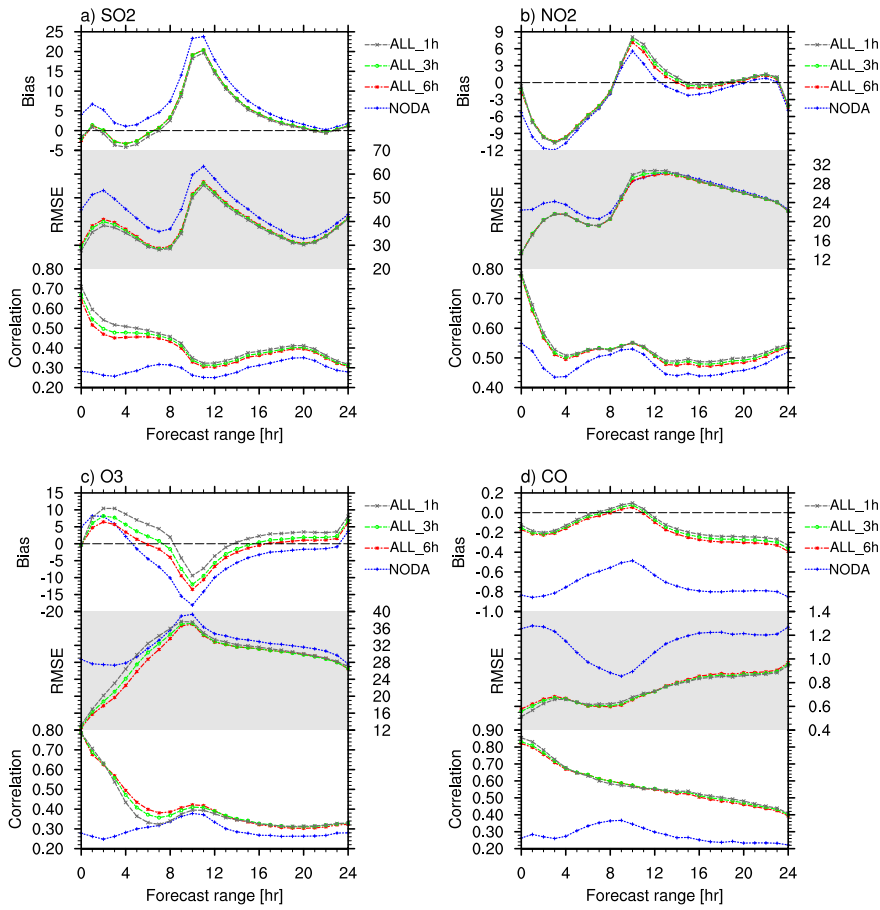
删除的内容: 8

删除的内容: 8



1370
 1371 **Figure 10.** Averaged bias (units: $\mu\text{g}/\text{m}^3$), RMSE (units: $\mu\text{g}/\text{m}^3$), and correlation for (a) PM_{2.5} and (b)
 1372 PM₁₀ in different experiments as a function of forecast range, verified against the surface observations
 1373 of 531 stations in China. The blue, red, green and gray lines denote the results of experiment NODA,
 1374 ALL_6h, ALL_3h, and ALL_1h, respectively.

删除的内容: 9

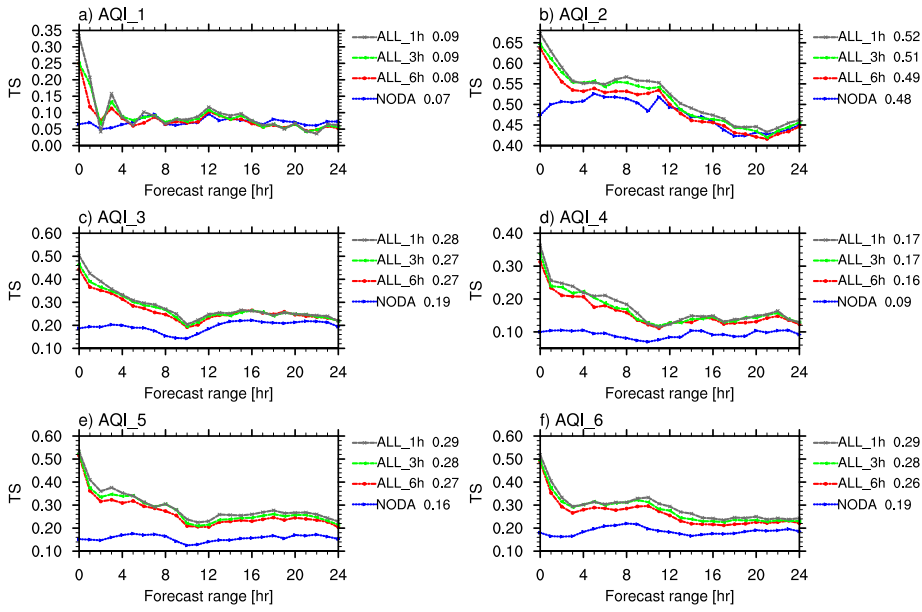


1376

1377 **Figure 11.** Same as Fig. 10, but for the forecast of (a) SO₂, (b) NO₂, (c) O₃ (units: μg/m³), and (d) CO

1378 (units: mg/m³).

删除的内容: 0
删除的内容: 9



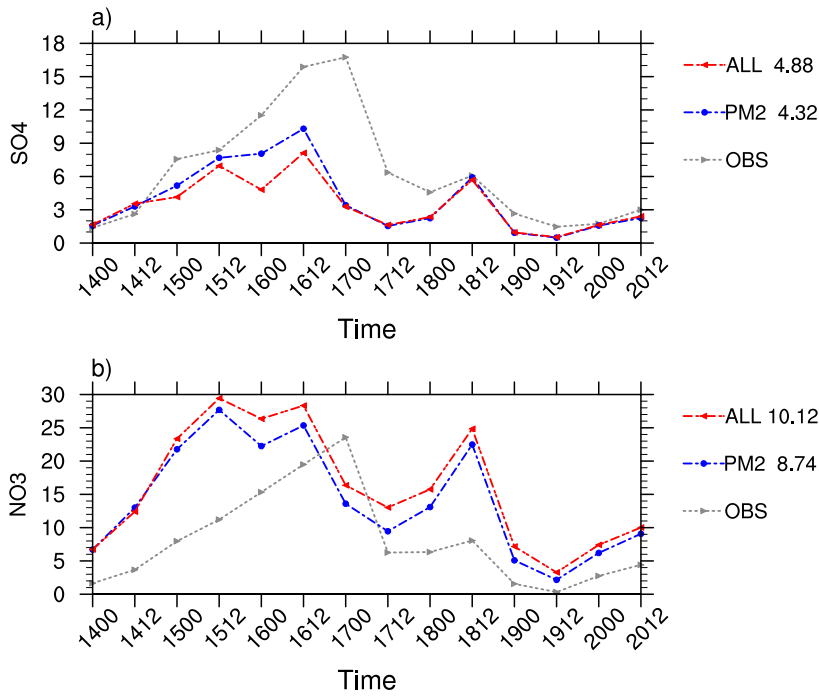
1381

1382

Figure 12. Same as Fig. 8, but for the experiments of NODA, ALL_6h, ALL_3h, ALL_1h, respectively.

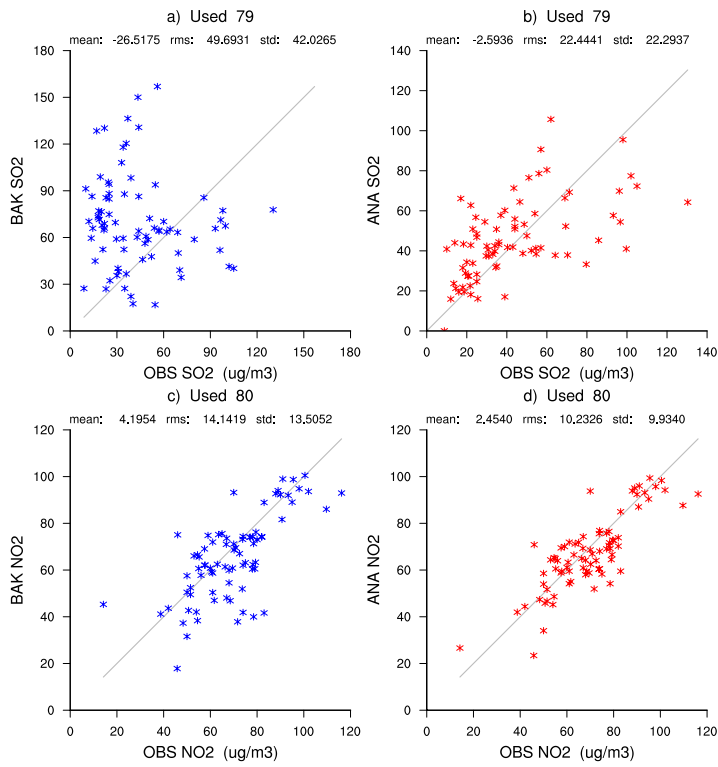
删除的内容: 1

删除的内容: 7



1385
 1386 **Figure 13.** Time series of (a) sulfate, (b) nitrate over January 14-20, verified against the size-resolved
 1387 particle observation at IUM station (units: $\mu\text{g}/\text{m}^3$). The gray, blue and red lines denote the observation
 1388 and the results of experiment PM2 and ALL, respectively. The numbers on the right of each panel
 1389 denote the averaged RMSE over January 14-20 for different experiments.

删除的内容: 2



1391

1392 **Figure 14.** Averaged scatter plot of (a, c) observation versus background and (b, d) observation versus
 1393 analysis for (a, b) SO₂ and (c, d) NO₂ around Beijing area (red dots in Fig. 1) on January 16. The
 1394 numbers on the title denote the accumulated numbers of the used observations around Beijing area
 1395 during January 16 (1600 UTC, 1606 UTC, 1612 UTC, and 1618 UTC).

删除的内容: 3

for O₃, although improvements are acquired at the 6-h cycling frequency, **the analysis at 00 UTC and 24-hr forecast (starting from 00 UTC) of O₃ becomes generally worse under higher cycling frequencies for this winter season, although biases did decrease at 09-14 UTC for 24-hr forecast. Considering the relevant NO_x-VOC-O₃ reaction system, changing the NO₂/O₃ concentration in a short period, the advantage of IC DA is competing with the disadvantage of the disordered photochemistry (inaccurate NO₂/VOC ratios) or changed titration (adjusted NO₂ concentrations but not NO) from the unadjusted VOC/NO and the updated O₃/NO₂ by DA. the advantage of more frequent IC DA could be consumed by the disordered photochemistry (inaccurate NO₂/VOC ratios) due to the unadjusted VOC and the updated O₃ and NO₂ from DA. In future applications, it is better to assimilate PM_{2.5}, PM₁₀, SO₂, and CO every 1 h. For the frequency of and assimilating O₃ and NO₂, every 6 h is the best in this winter season in our study. Since O₃ has strong diurnal and seasonal features, more experiments and statistics at different time of the day and different season of the year should be conducted in the future.** It might also be helpful to assimilate NO/VOC simultaneously with O₃ and NO₂ after there are corresponding measurements.